BETAINE HOMOCYSTEINE S-METHYLTRANSFERASE EMERGES AS A NEW PLAYER OF THE NUCLEAR METHIONINE CYCLE

Juliana Pérez-Miguelsanz[a,b], Néstor Vallecillo[a], Francisco Garrido[a], Edel Reytor[a], Dolores Pérez-Sala[c], María A. Pajares[a,d*]

[a]Instituto de Investigaciones Biomédicas Alberto Sols (CSIC-UAM), Arturo Duperier 4, 28029 Madrid, Spain.

[b]Departamento de Anatomía y Embriología Humanas, Facultad de Medicina, Universidad Complutense de Madrid, Plaza de Ramón y Cajal s/n, 28040 Madrid, Spain.

[c]Centro de Investigaciones Biológicas (CSIC), Ramiro de Maeztu 9, 28040 Madrid, Spain.

[d]Instituto de Investigación Sanitaria La Paz (IdiPAZ), Paseo de la Castellana 261, 28046 Madrid, Spain.

*To whom correspondence should be addressed at: Instituto de Investigaciones Biomédicas Alberto Sols (CSIC-UAM), Arturo Duperier 4, 28029 Madrid, Spain. (Phone: 34-915854414; FAX: 34-915854401; email: mapajares@iib.uam.es)

Running title: Acute liver failure and methionine metabolism.

Abbreviation list: AdoHcy, S-adenosylhomocysteine; AdoMet, S-adenosylmethionine; AGFC, analytical gel filtration chromatography; AHCY, S-adenosylhomocysteine hydrolase; APAP, acetaminophen; BHMT, betaine homocysteine methyltransferase; BSO, buthionine sulfoximine; EGSH, glutathione ethyl ester; Gal, D-galactosamine; GNMT, glycine N-methyltransferase; Hcy, homocysteine; H3K27me3, histone 3 lysine 27 trimethylation; MAT, methionine adenosyltransferase; NAC, N-acetylcysteine; NLS, nuclear localization signal; RTqPCR, real-time RT-PCR.

ABSTRACT

The paradigm of a cytoplasmic methionine cycle synthesizing/eliminating metabolites that are transported into/out of the nucleus as required has been challenged by detection of significant nuclear levels of several enzymes of this pathway. Here, we show betaine homocysteine S-methyltransferase (BHMT), an enzyme that exerts a dual function in maintenance of methionine levels and osmoregulation, as a new component of the nuclear branch of the cycle. In most tissues, low expression of *Bhmt* coincides with a preferential nuclear localization of the protein. Conversely, the liver, with very high *Bhmt* expression levels, presents a main cytoplasmic localization. Nuclear BHMT is an active homotetramer in normal liver, although the total enzyme activity in this fraction is markedly lower than in the cytosol. N-terminal basic residues play a role in cytoplasmic retention and the ratio of glutathione species regulates nucleocytoplasmic distribution. The oxidative stress associated with D-galactosamine (Gal) or buthionine sulfoximine (BSO) treatments induces BHMT nuclear translocation, an effect that is prevented by administration of N-acetylcysteine (NAC) and glutathione ethyl ester (EGSH), respectively. Unexpectedly, the hepatic nuclear accumulation induced by Gal associates with reduced nuclear BHMT activity and a trend towards increased protein homocysteinylation. Overall, our results support the involvement of BHMT in nuclear homocysteine remethylation, although moonlighting roles unrelated to its enzymatic activity in this compartment cannot be excluded.

Keywords: betaine homocysteine methyltransferase, subcellular localization, galactosamine intoxication, cytosolic retention, oxidative stress, one-carbon metabolism.

1. INTRODUCTION

Mammals obtain betaine from food (i.e. seafood, wheat germ or bran, spinach) or by mitochondrial choline oxidation [1, 2]. In hepatocytes, this reaction allows the recovery of one of the three methyl groups spent in choline/phosphatidylcholine biosynthesis by methylation of ethanolamine/phosphatidylethanolamine, using S-adenosylmethionine (AdoMet) as methyl donor [3]. Betaine has a dual cellular function, serving both as cellular osmolyte and as methyl donor for betaine homocysteine S-methyltransferase (BHMT) [4, 5]. In this last role, the enzyme methylates homocysteine (Hcy) for the synthesis of methionine and dimethylglycine. This is one of the two reactions of the methionine cycle that allow maintenance of methionine levels when the intake of this amino acid is reduced [5]. High AdoMet concentrations control remethylation by impairing this part of the methionine cycle through: i) reduction of *Bhmt* expression; ii) inhibition of the synthesis of 5-methyltetrahydrofolate, the methyl donor for the second Hcy remethylating enzyme, methionine synthase; and iii) activating the last steps of the trans-sulfuration pathway [5-7]. Conversely, under low methionine concentrations remethylation reactions are promoted to sustain adequate AdoMet synthesis, a process in which the higher Hcy affinity exhibited by BHMT and methionine synthase as compared to trans-sulfuration enzymes plays a key role [5, 8].

BHMTs are highly conserved homotetramers composed by subunits of 407 residues (rat), each containing a Zn^{2+} atom coordinated by three cysteines (C217, C299, C300) and a tyrosine (Y160) [9, 10]. Oxidation inhibits the enzyme activity inducing the release of Zn^{2+} and producing an intrasubunit disulfide bond between two active site cysteines [9, 11]. The structure of each subunit consists of a $(\alpha/\beta)_8$ barrel containing the active site and a C-terminal α-helix (~25 residues long) that holds together upper and lower subunits and *vice versa* forming a tight tetramer [9, 10]. This arrangement

contributes to the high stability exhibited by the enzyme against denaturants and temperature [12, 13].

BHMT has long been known as a cytosolic enzyme that represents ~1% of the total protein in hepatocytes [14, 15]. Although its highest levels have been found in human and rodent livers [14-16], BHMT has also been detected in kidney [14], eye lens [17] and cochlea [18]. Nonetheless, the high abundance of the protein in liver does not explain the comparatively low remethylating activity detected, thus suggesting its putative participation in additional functions (moonlighting). In fact, in the eye lens its structural role as ψ-crystallin was proposed [17].

Most regulatory studies on BHMT and the methionine cycle have been carried out in the cytoplasm, where key enzymes of this pathway were classically described [5, 6, 19]. However, there are dozens of methyltransferases that exhibit a variety of locations according to their function [20], and that therefore require the supply of AdoMet to their specific places, as well as the elimination of the S-adenosylhomocysteine (AdoHcy) produced. Due to the small size of these metabolites, their transport from the cytoplasm to the required compartment, and *vice versa*, was generally assumed, a view that was reinforced by the discovery of a mitochondrial AdoMet transporter [21]. However, in the last decades several authors described the presence of methionine adenosyltransferases (MATs) and S-adenosylhomocysteine hydrolase (AHCY) in the nucleus [22-26], thus challenging the former hypothesis and suggesting the need of a nuclear pool of these enzymes to sustain epigenetic methylations. Additionally, one of the main consumers of hepatic AdoMet, glycine N-methyltransferase (GNMT), has also been found in nuclear fractions, although its role in that compartment remains under debate [27]. More recently, our work demonstrated nuclear accumulation of MATα1, AHCY and GNMT in acute liver injury, higher levels

of the former correlating with increased histone 3 lysine 27 trimethylation (H3K27me3), a well-known repression mark [23]. Oxidative stress, and specifically glutathione levels and the GSH/GSSG ratio, control MATα1 subcellular distribution [23], but again no information about the rest of the enzymes of the methionine cycle exists. The present work now adds BHMT as a new player of the nuclear methionine metabolism and provides the first evidence of Hcy remethylation in this compartment. Moreover, our results involve the N-terminal basic residues of BHMT in cytoplasmic retention, and point to changes in glutathione levels as regulators of the nucleocytoplasmic distribution of the enzyme in acute liver injury.

2. MATERIALS AND METHODS

2.1. Constructions and mutagenesis. The pBS-BHMT plasmid reported by González et al. [28] was HindIII/BamHI digested and the insert cloned into pCMV4-FLAG (Sigma Chemical Co, St. Louis, MO, USA) to generate pFLAG-BHMT that contains a 6-residue linker (LDIEFH) between the FLAG-tag and the rat BHMT ORF. Elimination of the BHMT stop codon was performed in pBS-BHMT using the QuikChange method, the primer 5'-CAAATCCGCACAGCAGGGATCCACTAGTTC-3' and its complementary. This ORF was extracted by KpnI/BamHI digestion and cloned into pTRE-tight-EGFP (BD Bioscience, San Jose, CA, USA) to obtain the pTRE-tight-BHMT-EGFP plasmid. The resulting BHMT-EGFP fusion protein contained a C-terminal linker with the sequence QGSPP. This BHMT-EGFP insert was later cloned into the NdeI/HindIII sites of pT7.7, leading to pT7.7-BHMT-EGFP for *E. coli* expression. The pTRE-tight-BHMT-EGFP plasmid was also subjected to SacII/XhoI digestion to obtain the BHMT ORF lacking the stop codon, which was

cloned into pEGFP-N1 (BD Bioscience). The resulting pBHMT-EGFP plasmid codes for a BHMT-EGFP fusion protein including a 12-residue linker with the sequence GSPRARDPPVAT.

Site-directed mutagenesis was carried out on pFLAG-BHMT and pBHMT-EGFP for expression and analysis of the mutant proteins in mammalian cells, as well as in pTYB12-BHMT for heterologous expression and characterization of the purified protein forms [28]. For this purpose, the QuikChange method was used together with the following oligonucleotides (sense only): 5'-CCGATTGCCGGCGCGAAGGCCAAGAGG-3' (K7A); 5'-GATTGCCGGCAAGGCGGCCAAGAGGGG-3' (K8A); 5'-CCGGCAAGAAGGCCGCGAGGGGAATCTTAG-3' (K10A); 5'-GGCAAGAAGGCCAAGGCGGGAATCTTAGAACGC-3' (R11A). Sequences were verified by automatic sequencing at the Genomic Service of the Instituto de Investigaciones Biomédicas Alberto Sols (IIBM, CSIC-UAM).

2.2. Expression of the tagged BHMTs and purification of the recombinant proteins. Competent *E. coli* BL21(DE3) cells were transformed with pT7.7-BHMT-EGFP, pFLAG-BHMT or the mutated pTYB12-BHMT plasmids. Single colonies were grown at 37ºC in LBA media until A_{600} 0.6-0.8 was reached. IPTG 0.5 mM (Ambion, Austin TX, USA) was added to the cultures to induce expression from pT7.7 (3 hours at 37ºC) and pTYB12 plasmids (16 hours at 20ºC). The pFLAG plasmids, showing constitutive expression, were grown in parallel for the same time than pT7.7 plasmids. Cytosolic fractions from cells transformed with pTYB12 plasmids were obtained and used for the purification of recombinant proteins on chitin columns as previously described [28]. Samples of the purified proteins (7 μg) were loaded on SDS-PAGE 10% gels and stained with Coomassie blue.

2.3. Determination of BHMT and LDH activities. Purified proteins and cytosolic fractions (75 μl) were used to measure BHMT activity, as previously described [29]. Detection of BHMT activity in nuclear fractions required incubation for up to 2 hours and a standard reaction mixture containing ^{14}C-betaine (4 Ci/mol). Further enhancement of the radioactive specific activity in the reaction mixture resulted in a high background that precluded detection of nuclear BHMT activity, and hence the compromise achieved between a moderate increase in this parameter and extension of the reaction time. LDH activity was measured at 340 nm and 37ºC for 5 min using 10-100 μl of the subcellular fractions in 50 mM Tris/HCl pH 7.5, 0.2 mM NADH (Sigma) and 1 mM pyruvate (Sigma).

2.4. Analytical gel filtration chromatography (AGFC). Samples of cytosols (1 mg), nuclear fractions (400 μg) or purified proteins (5 μg) were loaded on a Superose 12 10/300 GL column (GE Healthcare, Barcelona, Spain) equilibrated and eluted at 0.3 ml/min in 50 mM Tris/HCl pH 8, 10 mM $MgSO_4$, 1 mM EDTA containing 150 mM KCl. Fractions (210 μl) were collected for activity measurements and dot-blot analyses. The markers (GE Healthcare and Sigma) used for column calibration were: blue dextran (2000 kDa), apoferritin (443 kDa), β-amylase (200 kDa), alcohol dehydrogenase (150 kDa), conalbumin (75 kDa), ovalbumin (43 kDa), carbonic anhydrase (29 kDa) and ATP (551 Da).

2.5. Western blotting and dot-blot. Samples of the purified recombinant proteins (5 μg), tissue cytosolic (80 μg or 15 μg for liver) and nuclear fractions (150 μg), cell cytosolic (25 μg) and nuclear fractions (50 μg) were loaded on SDS-PAGE 10% gels and electrotransferred to nitrocellulose membranes; 14% SDS-PAGE gels were used for detection of caspase-3 and protein homocysteinylation. Aliquots (150 μl) of the fractions collected from AGFC were used for dot-blot as previously described

[30]. Membranes were incubated with: rabbit anti-BHMT (1:20000 v/v) [28]; rabbit anti-caspase 3 (1:1000 v/v; Cell Signaling, Danvers, MA, USA) for evaluation of apoptosis; rabbit anti-Hcy (1:1000 v/v; Millipore, Temecula, CA, USA) for detection of protein homocysteinylation; mouse anti-α-tubulin (1:2500 v/v, Sigma) and rabbit anti-lamin B1 (1:1000 v/v; Abcam, Cambridge, United Kingdom) for detection of cross-contamination between subcellular fractions. Anti-rabbit-HRP (1:10000 v/v; BioRad, Hercules, CA, USA) was generally used, except for detection of BHMT in extrahepatic tissues (1:5000 v/v) and protein homocysteinylation (1:3000 v/v). Anti-mouse-HRP (GE Healthcare) was always used at 1:20000 (v/v). Protein bands were visualized with Western Lightning™ chemiluminescence reagent (Perkin Elmer, Waltham, MA, USA) and densitometric scanning of the images was carried out using ImageJ.

2.6. Animals and treatments. Male Wistar rats (180-200 g) were used for the extraction of a variety of tissues (N=3), including: spleen, heart, cerebellum, brain, liver, intestine, skeletal muscle, lung, pancreas, kidney, testis and the inferior cava vein. Tissues were divided in two portions that were immediately frozen in liquid nitrogen or included in formaldehyde 10% (v/v) and later embedded in paraffin for immunohistochemistry. Additional animal groups were used for acute treatments with i.p. injections of 400 mg/kg D-galactosamine hydrochloride (Gal; Sigma, N=25), 250 mg/kg acetaminophen (APAP; Sigma, N=10) or PBS (Gal controls, N=25; APAP controls N=10) as previously described [23]. Livers of the treated animals were processed immediately for subcellular fractionation, fixed or frozen in liquid nitrogen according to the requirements of subsequent procedures. Serum transaminase levels were determined at the Centro de Análisis Sanitarios of the Universidad Complutense de Madrid (Facultad de Farmacia, Madrid, Spain) and found to be significantly increased in Gal- and APAP-treated samples. AST levels were 28.33 ± 1.71 U/L in the

controls (N=6), 826.7 ± 282.8 U/L in Gal-treated animals (N=6; p=0.018) and 2946.0 ± 1191.3 U/L in APAP-treated rats (N=6; p=0.0002). ALT values were 131.5 ± 11.16 U/L, 1727.0 ± 524.4 U/L (p=0.012) and 1132 ± 520.4 U/L (p=0.0011), respectively. All animals received standard diets *ad libitum* and were sacrificed using CO_2 asphyxiation. The experiments included in this study were approved by the CSIC Bioethics Committee and carried out in full accordance with Spanish regulations (RD 53/2013) and the European Community guidelines (2010/63/EU) for the use of laboratory animals.

2.7. Subcellular fractionation. Tissue samples were homogenized in 4 volumes of 10 mM Tris/HCl pH 7.4, 0.3M sucrose, 0.1 mM EGTA, 0.1 % (v/v) 2-mercaptoethanol (Merck, Darmstadt, Germany), 1 mM benzamidine (Sigma), 2 mM PMSF (Sigma) and 10 μg/ml soybean trypsin inhibitor (Sigma) and centrifuged for 20 min at 12500 xg and 4ºC. The supernatants were collected and centrifuged at 105000 xg for 1 hour at 4ºC to obtain the cytosolic fractions. Separation of nuclear and cytoplasmic fractions was carried out in the absence of detergents as previously described [22, 31]. For this purpose, liver samples (~8 g) or H35 cells (2 $x10^6$/p100), wild type and transiently transfected with pFLAG-BHMT or the mutant plasmids, were used. Samples of subcellular fractions were utilized for western blotting, AGFC and activity determinations. Cross-contamination among fractions was monitored by measuring LDH activity and by densitometric scanning of the immunoblot signals for the marker proteins α-tubulin (cytoplasm) and lamin B1 (nucleus), as previously described [22].

2.8. Histology and immunohistochemistry. Paraffin sections were used for standard hematoxylin/eosin staining (10 μm) or immunohistochemistry (5 μm). In this last case, sections were incubated with anti-BHMT or preimmune rabbit sera (1:1000 v/v)[28], followed by EnVision (DAKO Corporation, Carpinteria, CA, USA) as

previously described [22]. Counterstaining was performed with hematoxylin. Sections were photographed and analyzed using Adobe-Photoshop CS software v. 8.0.1 (Adobe Systems Inc., San José, CA, USA).

2.9. RNA isolation and real-time RT-PCR (RTqPCR). Total RNA from rat tissues was isolated using the Tri-Reagent (Sigma) and treated with DNase following the manufacturer's instructions. RTqPCR was performed using the *Rn18s* gene as reference, the *Bhmt* primers and conditions previously described [32]. Calculations were carried out by the Pfaffl method [33].

2.10. Cell culture, transfections and treatments. Commercial CHO (Chinese hamster ovary), N2a (mouse neuroblastoma), COS-7 (monkey kidney) and H35 (rat hepatoma) cell lines were obtained from the ATCC and IIBM collections and grown in DMEM (Gibco, Carlsbad, CA, USA) supplemented with 10% (v/v) FBS and 2 mM glutamine. For CHO-K1 Tet-On cell line (BD Bioscience) culture, 10% (v/v) Tet system-approved FBS (BD Biosciences) was used. Transfections were performed using Lipofectamine (Invitrogen, Carlsbad, CA, USA). Selection of stable clones was performed in the Tet-On system using 1-1.4 mg/ml hygromycin (BD Biosciences) starting after 48 hours of culture. Doxycycline (BD Biosciences) dependence was analyzed in the range 0-4 μg/ml and one of the stable clones showing doxycycline-dependent expression of BHMT-EGFP was called CHO Tet-On BHMT-EGFP and used in further studies.

Cells were treated 48 hours with 10 mM Gal (Sigma) or 24 hours with 1 mM buthionine sulfoximine (BSO; Sigma) prior to subcellular fractionation [23]. These agents were used alone or in combination with compounds that serve as glutathione precursors, 5 mM N-acetylcysteine (NAC; Sigma), 0.5 mM AdoMet (Sigma) or 1 mM

glutathione ethyl ester (EGSH; Sigma) that were added to the culture 12 hours (NAC) or 15 min (AdoMet, EGSH) before Gal or BSO addition.

2.11. Confocal microscopy. Cells transiently overexpressing BHMT-EGFP, the BHMT-EGFP mutants and the CHO Tet-On BHMT-EGFP stable clone (in the presence of doxycycline) were grown on glass coverslips (50000-100000 cells) and fluorescence detected after 48 hours of culture. For immunofluorescence (20000-40000 cells), wild type cells or transiently transfected with FLAG-BHMT or the mutants were fixed for 10 minutes with 2% (v/v) formaldehyde, permeabilized for 10 minutes with 0.3% (v/v) Triton X-100 (Calbiochem, Darmstadt, Germany) and incubated for 30 minutes with 10% (v/v) FBS. Incubations with the primary antibodies, monoclonal M2 anti-FLAG antibody (5 μg/ml; Sigma) or polyclonal anti-BHMT (1:1000 v/v), were performed for 1 hour at RT. The corresponding secondary antibody, anti-mouse or anti-rabbit IgG conjugated to Alexa fluor 488 (1:800 v/v; Molecular Probes, Carlsbad, CA, USA), was added for 1 hour at RT. Glass coverslips were mounted using FluorSave™ reagent (Calbiochem). Nuclei were stained using 5 μg/ml Hoechst 33342 dye (Molecular Probes) for 1 hour before fixation or direct observation. Cell imaging (0.3-0.4 μm sections) was performed on a Leica TCS SPII Spectral microscope using a 63x/1.3 NA objective. Images were analyzed using the Leica Confocal Software (LCS Lite, Zurich, Switzerland).

2.12. Protein and glutathione concentrations. The protein concentration of the samples was measured using the Bio-Rad protein assay kit and bovine serum albumin as the standard. Glutathione concentrations (GSH and GSSG) and the GSH/GSSG ratio were measured in the H35 cells treated with different additives as previously described [23].

2.13. Sequence analysis and molecular modeling. Analysis of the rat BHMT sequence was performed using NetNES [34], PredictNLS [35] and PSort II servers.

2.14. Statistical analysis. Student's t-test for unpaired samples was applied for statistical analysis using GraphPad Prism v. 5.0 (GraphPad Software, San Diego, CA, USA). Differences were considered significant when $p \leq 0.05$.

3. RESULTS

3.1. *BHMT is a cytoplasmic and nuclear protein.*

The subcellular distribution of endogenous BHMT was analyzed in rat hepatoma H35 cells using a polyclonal anti-BHMT previously described (Fig. 1a). Confocal microscopy showed BHMT immunoreactivity mainly in the cytoplasm (C), but also in the cell nucleus (N). Western blotting of cytoplasmic and nuclear fractions of H35 cells also showed the presence of BHMT in both compartments (Fig. 1b). Further confirmation of these results was carried out by overexpression of BHMT forms that included a tag at either the N- (FLAG-BHMT) or C-terminal (BHMT-EGFP) ends of the protein, allowing immunofluorescence with monoclonal anti-FLAG or direct fluorescence detection, respectively. The influence of each tag on essential enzyme characteristics was assessed upon heterologous overexpression in *E. coli* using pFLAG-BHMT (constitutive expression) or pT7.7-BHMT-EGFP (IPTG induced). Both tagged proteins showed the expected size on western blotting (Fig. 2), exhibited BHMT activity and preserved the tetrameric association state (Table 1). Immunofluorescence (FLAG-BHMT) and direct fluorescence (BHMT-EGFP) observation by confocal microscopy were then performed upon transient transfection in several cell lines (Fig. 3a and 3b). Quantification of the protein distribution between compartments was

performed and the cells classified according to the calculated cytosolic to nuclear (C/N) signal ratio (Fig. 3c and 3d). Results with either FLAG-BHMT or BHMT-EGFP confirmed the presence of a strong cytoplasmic signal, but also BHMT localization to the cell nucleus. In fact, the BHMT-EGFP construct displayed a subcellular distribution pattern opposite to that of control EGFP (Fig. 3c). In order to verify that this phenomenon was not due to a saturation effect, a stable doxycycline-inducible BHMT-EGFP clone was prepared in CHO Tet-On cells. Induction with doxycycline concentrations above 1 μg/ml allowed detection of cytoplasmic and nuclear BHMT-EGFP by direct confocal microscopy (Fig. 4a and 4b). Analysis of cytosols from the stable clone showed BHMT expression already at 250 ng/ml doxycycline by western blotting (Fig. 4c).

This pattern of subcellular distribution resembles that previously described by our laboratory for MATα1 [22], being the nucleus the main localization in tissues other than the liver, where expression of this protein is minimal. Therefore, we performed RTqPCR to analyze the *Bhmt* expression level in a panel of rat tissues, taking testis levels as reference (Fig. 5a). As expected, maximal expression was detected in liver, followed by kidney, whereas low expression levels were found in other tissues such as testis, brain, lung, cerebellum and skeletal muscle. Western blotting analysis of the same panel of rat tissues confirmed previous results detecting BHMT only in liver and kidney cytosols (Fig. 5a). Immunohistochemistry was then performed in the whole panel of rat tissues using anti-BHMT and the corresponding preimmune serum (Fig. 5b). Nuclear staining was detected in several cell types and structures (Table 2), this localization being predominant in tissues with low expression levels such as the pancreas.

Next, liver subcellular fractions were isolated in the absence of detergents to characterize nuclear BHMT. The presence of the hepatic protein in both cytosolic and nuclear fractions was confirmed by western blotting, whereas no signal was detected in the washing step (S8) preceding nuclear protein extraction (Fig. 6a). Putative cross-contamination between cytoplasmic and nuclear fractions was evaluated by western blotting and no nuclear tubulin signal was detected (Fig. 6a). Additionally, the presence of cytoplasmic contamination was also ruled out by measuring LDH activity, which was found to be <0.1 % in all the nuclear fractions isolated. Nuclear BHMT was able to synthesize methionine from Hcy and betaine, although the total activity was ~300 fold lower in the nucleus than in the cytosol, as expected from the small amount of enzyme found in the nuclear fraction (Fig. 6b). The nuclear specific activity calculated using the total protein concentration was 41.60 ± 9.79 pmol/min/mg (N=5), representing ~10% of that in the cytoplasm (439.00 ± 91.19 pmol/min/mg; N=5). However, the abundance of BHMT in each fraction as compared to the total protein content is dramatically different, and this fact has a direct influence in the specific activity obtained. Therefore, the specific activity was recalculated using the signal for the BHMT specific band obtained by western blotting. In this case, the values were 1.32 ± 0.36 nmol/min/A.U. for the cytosolic protein and 0.92 ± 0.49 nmol/min/A.U. for the nuclear BHMT, thus indicating lack of significant differences. Moreover, analysis of the association state of nuclear BHMT by AGFC demonstrated preservation of the tetrameric assembly according to its elution volume and as expected for the active form of the enzyme (Fig. 6c).

3.2. *Subcellular distribution of BHMT in acute liver injury.*

The nucleocytoplasmic distribution of several enzymes of methionine metabolism is altered in liver disease. Therefore, we examined whether BHMT

localization is also perturbed under pathological situations, namely acute Gal-intoxication, initially in H35 cells. Confocal microscopy revealed alterations in the distribution of the endogenous protein using anti-BHMT in Gal-treated cells (Fig. 7a). Quantification of the results demonstrated a decrease in the cytoplasmic signal, together with an increase in nuclear fluorescence (Fig. 7b). Similarly, nuclear accumulation was also observed in cells overexpressing BHMT-EGFP after Gal-treatment (Fig. 7c), although in this case the changes were more moderate (Fig. 7d). Noteworthy, addition of Gal did not affect EGFP distribution. Moreover, subcellular fractionation of control and treated H35 cells followed by western blotting confirmed a significant decrease in cytosolic BHMT ($p=0.036$), together with nuclear accumulation ($p=0.007$) after Gal treatment (Fig. 8a).

The pathophysiological significance of these observations was further evaluated using a rat model of Gal-induced acute liver injury. Immunohistochemical analysis of liver sections of control and treated rats using anti-BHMT and the corresponding preimmune serum showed a decrease in the cytoplasmic signal and confirmed accumulation of BHMT in the nucleus of Gal-treated livers (Fig. 8b). The hepatic subcellular fractions of Gal-treated rats compared to those of control livers showed a significant reduction in BHMT specific activity, the decrease being 25% in the cytosol ($p=0.042$) and reaching 50% in nuclear factions ($p=0.047$) (Fig. 9a). This change in nuclear BHMT activity correlated with alterations in global protein homocysteinylation as shown by western blotting (Fig. 9b). Densitometric scanning indicated a trend towards increased anti-Hcy signals in Gal-treated samples (0.56 ± 0.15) as compared to the controls (0.33 ± 0.11, $p=0.09$) after normalization with lamin B1 levels. Cytosolic BHMT levels and activity followed a similar pattern, decreasing in Gal-treated livers (Fig. 9c). In contrast, the decline in nuclear activity coincided with BHMT

accumulation in Gal-treated samples, suggesting loss of activity of nuclear BHMT (Fig. 9c). No changes in the AGFC elution profile of nuclear BHMT were detected between control and Gal-treated samples (Fig. 9d), and hence the reduced activity did not correlate with dissociation or aggregation.

Among others, oxidative stress could have a role in the changes of BHMT subcellular distribution induced by Gal. To explore this possibility, H35 cells were treated for 48 hours with Gal alone or after preincubation with glutathione precursors, NAC or AdoMet. Glutathione concentrations were measured in H35 cells and found to decrease by ~50% after Gal-treatment (Fig. 10a), a similar change being detected in the GSH/GSSG ratio (Fig. 10b). This reduction in GSH levels was prevented by preincubation with NAC but not with AdoMet, as previously described [23]. Similarly, changes in the GSH/GSSG ratio were precluded by NAC, but not by AdoMet. The effect of these compounds on the subcellular distribution of BHMT was then studied by western blotting of the cytosolic and nuclear fractions. As shown in liver, Gal treatment reduced the BHMT content of the cytosol (Fig.11a). NAC increased cytosolic BHMT levels, whereas preincubation with this agent prevented the decrease in enzyme levels induced by Gal treatment in this compartment (Fig. 11a). In contrast, AdoMet addition did not overcome Gal-effects and, in fact, this agent alone decreased cytosolic BHMT levels (Fig. 11a). Further confirmation of the putative role of glutathione levels in BHMT subcellular distribution was obtained through inhibition of glutathione synthesis with BSO. As previously described, a 95% reduction in GSH concentration was detected after 24 hours of treatment, together with a severe decrease in the GSH/GSSG ratio (Fig 10a,b). These changes correlated with diminished cytosolic BHMT levels and were prevented by the glutathione precursor EGSH, but not by AdoMet (Fig. 11b). Regarding nuclear BHMT levels, both NAC and AdoMet had no effect on this

parameter, but were able to preclude the Gal-induced nuclear accumulation of BHMT (Fig. 11c). BSO treatment also increased BHMT nuclear levels, an effect that EGSH administration tended to avoid ($p=0.07$), whereas AdoMet failed to do so (Fig. 11d). The potential toxicity of the treatments employed was assessed following induction of apoptosis through detection of the proteolytic cleavage of caspase-3 by western blotting. No signal of the proteolytic 17 kDa fragment was detected in any of the treated samples (Fig. 10c). Moreover, during microscopic analysis of the treated cells no signs of chromatin condensation, alteration of the plasma membrane integrity or the presence of apoptotic bodies were observed. Altogether these results suggested a role for glutathione ratios in the regulation of BHMT nucleocytoplasmic distribution.

Acute liver injury associated with severe GSH depletion is also produced by acetaminophen (APAP) overdose. Therefore, we also examined putative effects on hepatic BHMT subcellular distribution 24 hours after such treatment. GSH concentrations were reduced ~40% (15271.8 ± 3320.7 pmol/mg protein) by APAP as compared to control values (8214.99 ± 1746.33 pmol/mg protein; $p=0.008$), whereas the decrease in the GSH/GSSG ratio was ~25% and barely significant ($p=0.05$). In this case, no significant changes were detected in cytosolic BHMT levels, whereas a tendency towards decreased nuclear BHMT content was observed (Fig. 12a). Again, both cytosolic and nuclear BHMTs behaved as expected for tetramers in AGFC (Fig. 12b-e).

3.3. *BHMT N-terminal sequence is involved in cytoplasmic retention.*

The rat BHMT amino acid sequence was analyzed using NetNES, PredictNLS and the PSort II servers, in search for motifs that govern its subcellular localization. None of them identified a consensus sequence for nuclear localization (NLS), although they suggested ~22% of the protein in the nucleus. Having no clue as to which areas

may be involved in the control of BHMT subcellular distribution and given the fact that classical motifs involve basic residues, we decided to analyze the presence of such residues in the sequence and molecular surface of this enzyme. The BHMT N-terminal sequence (~10 residues) is part of a flexible area that was not solved in the crystal structure (Fig. 13a), and that contains four basic residues (^{7}KKAKR^{11}) in an arrangement similar to that of a monopartite NLS (Fig. 13b). This basic stretch is preserved in BHMTs according to BLASTP alignment, although conservative changes may take place, such as the replacement of arginine by lysine at position 11 of the human enzyme (Fig. 13c). Therefore, these residues were changed to alanine and the effect of the substitutions in enzyme activity and association state of the purified mutants was analyzed after their heterologous overexpression in *E. coli* using pTYB12 plasmids (Fig. 14). The use of this plasmid allowed purification on chitin columns using the N-terminal tag containing intein plus a chitin binding domain that remains attached to the column upon excision by incubation with reducing agents. All the mutant proteins were tetramers able to synthesize methionine, although K8A and K10A exhibited ~30% of the wild type activity (Table 3).

The effect of the mutations on BHMT subcellular distribution was analyzed in transiently transfected cells (H35 and CHO) using the FLAG- and EGFP-tagged constructs both by direct confocal microscopy (Fig. 15a) and immunofluorescence (Fig. 15b). Quantification of the images showed that the mutations lead to increased nuclear fluorescence as indicated by significant rises in the number of cells with either similar cytosolic and nuclear levels (C/N ratios 1.2 ± 0.2) or higher nuclear levels (C/N ratios <0.8). Similar results were also observed in transiently transfected CHO cells. These changes of distribution pattern were consistent for FLAG- and EGFP-tagged K8A and

K10A mutants, suggesting the involvement of these lysine residues in cytoplasmic retention (Fig. 15c and 15d**)**.

4. DISCUSSION

BHMT is involved in two key processes, maintenance of methionine levels to sustain AdoMet synthesis and osmoregulation by controlling betaine concentrations. Both roles are coupled in a single reaction and are essential in liver, where up to 50% of transmethylation reactions take place and urea concentrations may become harmful [20, 36]. Thus, the need of high *Bhmt* expression in liver is justified by both aspects, whereas its osmoregulatory function may become more important to explain *Bhmt* expression in organs such as the kidney, eye lens or cochlea that require a strict control of ionic levels [4, 37-39]. In fact, osmotic deregulation is the underlying cause of pathologies in these organs, including cataract development and deafness that are related to osmotic swelling and impairment of the endocochlear potential, respectively [37-39]. Results of RTqPCR of rat tissues now extend the list of organs exhibiting a certain level of *Bhmt* expression to the testis, brain, lung, skeletal muscle and cerebellum. Among them, the muscle exerts an indirect role in osmoregulation as sodium storage, whereas the lung can be considered an excretory organ and, as such, in need to control water and ion exchange [40]. In fact, abnormal hydration and osmotic pressure by mucus may contribute to chronic bronchitis [41]. In fish testis, impaired osmoregulation may affect sperm quality/motility indirectly through changes in mitochondrial function [42]. The rat *Bhmt* expression profile obtained by RTqPCR coincides with human and mouse data in their high hepatic levels, while kidney levels parallel those reported in mice [43]. However, differences were encountered among tissues with low expression levels, where human and mouse testis and cerebellum lack

Bhmt expression, whereas human and bat brain, and mouse lung and muscle exhibit significant *Bhmt* levels [43, 44].

Our immunohistochemistry data also differ from previous reports that only found cytoplasmic BHMT staining [45, 46]. Precisely, rat tissues with low *Bhmt* expression show the protein manly located to the cell nucleus, a distribution not observed before. In kidney, our results confirm BHMT in the cytoplasm of proximal tubules [45], but also demonstrate nuclear staining in this structure. However, no BHMT signal was observed in the distal tubules and collecting ducts, in contrast to data of Delgado-Reyes et al. [45]. Liver sections present BHMT labeling in the cytoplasm and nucleus of hepatocytes, this last compartment showing a weaker staining that was confirmed by western blotting. Previous work detected hepatic cytoplasmic staining [45], whereas BHMT was also noticed in hepatic canalicular and low basolateral membranes by western blotting [46], but again no nuclear BHMT was reported. Moreover, hepatic BHMT distribution was found to be homogeneous in human and pig, whereas a gradient with high periportal levels was described in rat [45]. However, in our immunohistochemistry images such a gradient was not evident, neither observed in Gal-treated livers. These disparities may arise from the use of different antibodies raised against BHMTs prepared with alternative protocols that may render diverse quality/purity of the antigens utilized for inoculation.

Bhmt expression and cytosolic protein levels are reduced in liver disease [23, 47, 48], effects that are further extended to liver and kidney upon high sodium intakes [49]. Here, we also show that in acute liver injury induced by Gal intoxication there is an opposite outcome in BHMT levels between cytosolic and nuclear compartments, decreasing in the former while increasing in the later. This effect resembles MATα1 behavior in the same model, whereas AHCY levels are only modified in the nucleus,

where their enhancement is detected [23]. As for MATα1 [22, 23], hepatic nuclear BHMT activity is much lower than in the cytoplasm, reflecting the different abundance of the enzymes in each compartment. However, when this fact is taken into account for the evaluation of the specific activity, similar values are obtained for both cytoplasmic and nuclear enzymes. BHMT, independently of its subcellular localization, requires betaine as methyl donor to catalyze Hcy remethylation, its source being either the diet or the mitochondrial oxidation of choline [5]. In either case, the small size of betaine allows its transport through the nuclear pore in order to supply the required amount of substrate for nuclear BHMT. Based on new data regarding BHMT affinity for betaine (K_m 75 μM) [50], this amount of methyl donor needed could be less than expected, and hence easily obtained through the nuclear pore. Additionally, the putative role of nuclear BHMT in Hcy remethylation can be also inferred from the increase in global protein homocysteinylation observed in Gal-treated samples, where nuclear BHMT accumulation correlates with reduced activity which, in turn, may lead to enhanced Hcy levels.

Our results also show that nuclear accumulation of BHMT depends on the decrease of glutathione concentrations and the GSH/GSSG ratio, effects that were induced both by Gal and BSO. Similar outcomes on subcellular distribution were previously reported for MATα1 upon alteration of the GSH/GSSG levels by these same compounds, but also by APAP [23]. Surprisingly, BHMT subcellular distribution is not significantly modified by APAP intoxication, despite the change induced in GSH levels. A putative explanation for this outcome may derive from the ability to modify proteins exhibited by the APAP metabolite NAPQI [51], which could block nuclear transport of BHMT. It is also known that BHMT activity is sensitive to oxidative stress, which leads to active site disulfide formation and loss of the essential Zn^{2+} atom [9, 11, 52]. Such

effects could be induced by Gal intoxication both in the cytoplasmic and nuclear BHMT pools, thus explaining the reduced activity measured in both compartments. Moreover, the addition of post-translational modifications such as nitrosylation or carbonylation [53, 54], reported to occur in BHMT, may also contribute to the decreased remethylation observed.

Examination of the BHMT sequence for the presence of consensus motifs involved in its nucleocytoplasmic transport rendered no information. However, basic residues have been involved in this type of transport and the BHMT sequence shows a small cluster of such amino acids at the N-terminal that is partially solved in the crystal structure [9, 10]. Elimination of the positive charge at these positions indeed demonstrated their role in cytoplasmic retention. Some of these lysine residues, including K7 and K10, are targets for post-translational modifications such as acetylation and trimethylation, which may be involved in BHMT localization. In fact, these modifications have been found in autophagy [55].

The presence of BHMT, MATs and AHCY in the nucleus suggests the existence of a small pool of methionine metabolism enzymes in this compartment in order to guarantee essential methylation events to sustain cell viability. In this line, nuclear MATs will provide AdoMet for epigenetic methylations, while AHCY will eliminate their inhibitor AdoHcy, and BHMT may recycle Hcy back to methionine to sustain AdoMet synthesis. This hypothesis is supported by results in several models showing the correlation between MAT activity and H3K27me3 [22, 23, 56] and AHCY activity and efficient cap methylation [26]. Results on acute liver injury also show nuclear accumulation of MATα1 and AHCY that parallels enhanced H3K27me3 [23], but this pattern is not followed by BHMT activity. In this case, enhanced protein levels correlate with reduced Hcy remethylation and a trend towards increased global

homocysteinylation. These results suggest a rise in nuclear Hcy levels and, in turn, those of the thiolactone that is involved in protein N-homocysteinylation, a modification related to protein aggregation and loss of function [57, 58]. The existence of this modification in nuclear proteins has been described, for example, in histone 3, and shown to influence its methylation levels, since both modifications share lysine as their target residue [59].

Another possibility to explain the presence of BHMT in the nucleus, independent from the low activity detected in this compartment, is related to its high stability and a putative role as structural protein, as previously proposed in the eye lens [12, 17]. In this case, BHMT could serve as the scaffold for other enzymes of the cycle to perform their function or even exert a moonlighting function. In fact, several enzymes of the intermediary metabolism have been proposed to exhibit alternative roles in different subcellular compartments [60].

Altogether, the available data suggest the existence of a nuclear methionine cycle in normal hepatocytes and a need for its reinforcement under pathological conditions. The normal levels of this nuclear pool may provide the substrate supply required for epigenetic methylations taking place continuously in every cell, but may not be enough to satisfy the requirements for epigenetic remodeling to respond against an insult (e.g. drug intoxication). This may result in the nuclear accumulation of methionine cycle enzymes in an attempt to fulfill this demand. However, protein modifications introduced, e.g. during oxidative stress, may result in the transport of inactive proteins, in alterations of protein-protein interaction patterns, or in moonlighting activities precluding the desired outcome. This seems the case of the nuclear accumulation of BHMT induced by Gal and the lack of effects due to APAP.

5. ACKNOWLEDGEMENTS

The authors wish to thank Mrs. A. Cerro and D. Arroyo for their technical assistance with histology. This work was supported by grants of the Ministerio de Economía y Competitividad (BFU2008-00666 and BFU2009-08977 to MAP; SAF2012-36519 and SAF2015-68590R to DPS) and Instituto de Salud Carlos III (RETIC RIRAAF RD12/0013/0008 and ARADYAL RD16/0006/0021 to DPS).

THE FUNDING BODIES HAD NO ROLE IN STUDY DESIGN, COLLECTION, ANALYSIS AND INTERPRETATION OF THE DATA, IN WRITING THE MANUSCRIPT OR IN THE DECISION TO SUBMIT FOR PUBLICATION.

6. REFERENCES

[1] Craig SA (2004) Betaine in human nutrition. Am J Clin Nutr 80:539-549

[2] Zeisel SH, Story DL, Wurtman RJ, Brunengraber H (1980) Uptake of free choline by isolated perfused rat liver. Proc Natl Acad Sci USA 77:4417-4419

[3] Noga AA, Stead LM, Zhao Y, Brosnan ME, Brosnan JT, Vance DE (2003) Plasma homocysteine is regulated by phospholipid methylation. J Biol Chem 278:5952-5955

[4] Garcia-Perez A, Burg MB (1991) Renal medullary organic osmolytes. Physiol Rev 71:1081-1115

[5] Pajares MA, Perez-Sala D (2006) Betaine homocysteine S-methyltransferase: just a regulator of homocysteine metabolism? Cell Mol Life Sci 63:2792-2803

[6] Mato JM, Alvarez L, Ortiz P, Pajares MA (1997) S-adenosylmethionine synthesis: molecular mechanisms and clinical implications. Pharmacol Ther 73:265-280

[7] Castro C, Breksa API, Salisbury EM, Garrow TA (2001) Betaine-homocysteine S-methyltransferase (BHMT) transcription is inhibited by S-adenosylmethionine (AdoMet). In: Milstien S, Kapatos G, Levine RA, Shane B (eds) Chemistry and Biology of Pteridines and Folates. Kluwer, Norwell MA, pp 549-556

[8] Finkelstein JD, Martin JJ (1984) Methionine metabolism in mammals. Distribution of homocysteine between competing pathways. J Biol Chem 259:9508-9513

[9] Evans JC, Huddler DP, Jiracek J, Castro C, Millian NS, Garrow TA, Ludwig ML (2002) Betaine-homocysteine methyltransferase: zinc in a distorted barrel. Structure 10:1159-1171

[10] Gonzalez B, Pajares MA, Martinez-Ripoll M, Blundell TL, Sanz-Aparicio J (2004) Crystal structure of rat liver betaine homocysteine s-methyltransferase reveals new oligomerization features and conformational changes upon substrate binding. J Mol Biol 338:771-782

[11] Miller CM, Szegedi SS, Garrow TA (2005) Conformation-dependent inactivation of human betaine-homocysteine S-methyltransferase by hydrogen peroxide in vitro. Biochem J 392:443-448

[12] Garrido F, Gasset M, Sanz-Aparicio J, Alfonso C, Pajares MA (2005) Rat liver betaine-homocysteine S-methyltransferase equilibrium unfolding: insights into intermediate structure through tryptophan substitutions. Biochem J 391:589-599

[13] Gonzalez B, Pajares MA, Too HP, Garrido F, Blundell TL, Sanz-Aparicio J (2002) Crystallization and preliminary X-ray study of recombinant betaine-homocysteine S-methyltransferase from rat liver. Acta Crystallogr D Biol Crystallogr 58.1507-1510

[14] McKeever MP, Weir DG, Molloy A, Scott JM (1991) Betaine-homocysteine methyltransferase: organ distribution in man, pig and rat and subcellular distribution in the rat. Clin Sci (Lond) 81:551-556

[15] Garrow TA (1996) Purification, kinetic properties, and cDNA cloning of mammalian betaine-homocysteine methyltransferase. J Biol Chem 271:22831-22838

[16] Yamashita T, Hashimoto S, Kaneko S, Nagai S, Toyoda N, Suzuki T, Kobayashi K, Matsushima K (2000) Comprehensive gene expression profile of a normal human liver. Biochem Biophys Res Commun 269:110-116

[17] Rao PV, Garrow TA, John F, Garland D, Millian NS, Zigler JS Jr (1998) Betaine-homocysteine methyltransferase is a developmentally regulated enzyme crystallin in rhesus monkey lens. J Biol Chem 273:30669-30674

[18] Martinez-Vega R, Garrido F, Partearroyo T, Cediel R, Zeisel SH, Martinez-Alvarez C, Varela-Moreiras G, Varela-Nieto I, Pajares MA (2015) Folic acid deficiency induces premature hearing loss through mechanisms involving cochlear oxidative stress and impairment of homocysteine metabolism. FASEB J 29:418-432

[19] Pajares MA, Markham GD (2011) Methionine adenosyltransferase (s-adenosylmethionine synthetase). Adv Enzymol Relat Areas Mol Biol 78:449-521

[20] Cantoni GL (1975) Biological methylation: selected aspects. Annu Rev Biochem 44: 435-451

[21] Agrimi G, Di Noia MA, Marobbio CM, Fiermonte G, Lasorsa FM, Palmieri F (2004) Identification of the human mitochondrial S-adenosylmethionine transporter: bacterial expression, reconstitution, functional characterization and tissue distribution. Biochem J 379:183-190

[22] Reytor E, Perez-Miguelsanz J, Alvarez L, Perez-Sala D, Pajares MA (2009) Conformational signals in the C-terminal domain of methionine adenosyltransferase I/III determine its nucleocytoplasmic distribution. FASEB J 23:3347-3360

[23] Delgado M, Garrido F, Perez-Miguelsanz J, Pacheco M, Partearroyo T, Perez-Sala D, Pajares MA (2014) Acute Liver Injury Induces Nucleocytoplasmic Redistribution of Hepatic Methionine Metabolism Enzymes. Antioxid Redox Signal 20:2541-2554

[24] Katoh Y, Ikura T, Hoshikawa Y, Tashiro S, Ito T, Ohta M, Kera Y, Noda T, Igarashi K (2011) Methionine adenosyltransferase II serves as a transcriptional corepressor of Maf oncoprotein. Mol Cell 41:554-566

[25] Radomski N, Barreto G, Kaufmann C, Yokoska J, Mizumoto K, Dreyer C (2002) Interaction of S-adenosylhomocysteine hydrolase of Xenopus laevis with mRNA(guanine-7-)methyltransferase: implication on its nuclear compartmentalisation and on cap methylation of hnRNA. Biochim Biophys Acta 1590:93-102

[26] Radomski N, Kaufmann C, Dreyer C (1999) Nuclear accumulation of S-adenosylhomocysteine hydrolase in transcriptionally active cells during development of Xenopus laevis. Mol Biol Cell 10:4283-4298

[27] Krupenko NI, Wagner C (1997) Transport of rat liver glycine N-methyltransferase into rat liver nuclei. J Biol Chem 272:27140-27146

[28] Gonzalez B, Campillo N, Garrido F, Gasset M, Sanz-Aparicio J, Pajares MA (2003) Active-site-mutagenesis study of rat liver betaine-homocysteine S-methyltransferase. Biochem J 370:945-952

[29] Finkelstein JD, Mudd SH (1967) Trans-sulfuration in mammals. The methionine-sparing effect of cystine. J Biol Chem 242:873-880

[30] Sanchez-Perez GF, Gasset M, Calvete JJ, Pajares MA (2003) Role of an intrasubunit disulfide in the association state of the cytosolic homo-oligomer methionine adenosyltransferase. J Biol Chem 278:7285-7293

[31] Andrews NC, Faller DV (1991) A rapid micropreparation technique for extraction of DNA-binding proteins from limiting numbers of mammalian cells. Nucleic Acids Res 19:2499

[32] Delgado M, Perez-Miguelsanz J, Garrido F, Rodriguez-Tarduchy G, Perez-Sala D, Pajares MA (2008) Early effects of copper accumulation on methionine metabolism. Cell Mol Life Sci 65:2080-2090

[33] Pfaffl MW (2001) A new mathematical model for relative quantification in real-time RT-PCR. Nucleic Acids Res 29:e45

[34] la Cour T, Kiemer L, Molgaar A, Gupta R, Skriver K, Brunak S (2004) Analysis and prediction of leucine-rich nuclear export signals. Protein Eng Des Sel 17:527-536

[35] Cokol M, Nair R, Rost B (2000) Finding nuclear localization signals. EMBO Rep 1: 411-415

[36] Coelho-Sampaio T, Ferreira ST, Castro Junior EJ, Vieyra A (1994) Betaine counteracts urea-induced conformational changes and uncoupling of the human erythrocyte Ca2+ pump. Eur J Biochem 221:1103-1110

[37] Kinoshita JH (1974) Mechanisms initiating cataract formation. Proctor Lecture. Invest Ophthalmol 13:713-724

[38] Tran BH (2002) Endolymphatic deafness: a particular variety of cochlear disorder. ORL J Otorhinolaryngol Relat Spec 64:120-124

[39] Zdebik AA, Wangemann P, Jentsch TJ (2009) Potassium ion movement in the inner ear: insights from genetic disease and mouse models. Physiology 24:307-316 doi: 10.1152/physiol.00018.2009

[40] Titze J (2015) A different view on sodium balance. Curr Opin Nephrol Hypertens 24:14-20 doi: 10.1097/MNH.0000000000000085.

[41] Anderson WH, Coakley RD, Button B, Henderson AG, Zeman KL, Alexis NE, Peden DB, Lazarowski ER, Davis CW, Bailey S, Fuller F, Almond M, Qaqish B, Bordonali E, Rubinstein M, Bennett WD, Kesimer M, Boucher RC (2015) The Relationship of Mucus Concentration (Hydration) to Mucus Osmotic Pressure and Transport in Chronic Bronchitis. Am J Respir Crit Care Med 192:182-190 doi: 10.1164/rccm.201412-2230OC

[42] Avarre JC, Guinand B, Dugue R, Cosson J, Legendre M, Panfili J, Durand JD (2014) Plasticity of gene expression according to salinity in the testis of broodstock and F1 black-chinned tilapia, Sarotherodon melanotheron heudelotii. PeerJ 2:e702 doi: 10.7717/peerj.702

[43] Chen NC, Yang F, Capecci LM, Gu Z, Schafer AI, Durante W, Yang XF, Wang H (2010) Regulation of homocysteine metabolism and methylation in human and mouse tissues. FASEB J 24:2804-2817

[44] Zhang Y, Zhu T, Wang L, Pan YH, Zhang S (2013) Homocysteine homeostasis and betaine-homocysteine S-methyltransferase expression in the brain of hibernating bats. PloS ONE 8:e85632

[45] Delgado-Reyes CV, Wallig MA, Garrow TA (2001) Immunohistochemical detection of betaine-homocysteine S-methyltransferase in human, pig, and rat liver and kidney. Arch Biochem Biophys 393:184-186

[46] Sehayek E, Wang R, Ono JG, Zinchuk VS, Duncan EM, Shefer S, Vance DE, Ananthanarayanan M, Chait BT, Breslow JL (2003) Localization of the PE methylation pathway and SR-BI to the canalicular membrane: evidence for apical PC biosynthesis

that may promote biliary excretion of phospholipid and cholesterol. J Lipid Res 44:1605-1613

[47] Forestier M, Banninger R, Reichen J, Solioz M (2003) Betaine homocysteine methyltransferase: gene cloning and expression analysis in rat liver cirrhosis. Biochim Biophys Acta 1638:29-34

[48] Avila MA, Berasain C, Torres L, Martin-Duce A, Corrales FJ, Yang H, Prieto J, Lu SC, Caballeria J, Rodes J, Mato JM (2000) Reduced mRNA abundance of the main enzymes involved in methionine metabolism in human liver cirrhosis and hepatocellular carcinoma. J Hepatol 33:907-914

[49] Delgado-Reyes CV, Garrow TA (2005) High sodium chloride intake decreases betaine-homocysteine S-methyltransferase expression in guinea pig liver and kidney. Am J Physiol 288:R182-187

[50] Mladkova J, Hladilkova J, Diamond CE, Tryon K, Yamada K, Garrow TA, Jungwirth P, Koutmos M, Jiracek J (2014) Specific potassium ion interactions facilitate homocysteine binding to betaine-homocysteine S-methyltransferase. Proteins 82:2552-2564 doi: 10.1002/prot.24619

[51] Baillie TA, Rettie AE (2011) Role of biotransformation in drug-induced toxicity: influence of intra- and inter-species differences in drug metabolism. Drug Metab Pharmacokinet 26:15-29

[52] Castro C, Millian NS, Garrow TA (2008) Liver betaine-homocysteine S-methyltransferase activity undergoes a redox switch at the active site zinc. Arch Biochem Biophys 472:26-33

[53] Lopez-Sanchez LM, Corrales FJ, Barcos M, Espejo I, Munoz-Castaneda JR, Rodriguez-Ariza A (2010) Inhibition of nitric oxide synthesis during induced

cholestasis ameliorates hepatocellular injury by facilitating S-nitrosothiol homeostasis. Lab Invest 90:116-127 doi: 10.1038/labinvest.2009.104.

[54] Newton BW, Russell WK, Russell DH, Ramaiah SK, Jayaraman A (2009) Liver proteome analysis in a rodent model of alcoholic steatosis. J Proteome Res 8:1663-1671

[55] Overbye A, Saetre F, Hagen LK, Johansen HT, Seglen PO (2011) Autophagic activity measured in whole rat hepatocytes as the accumulation of a novel BHMT fragment (p10), generated in amphisomes by the asparaginyl proteinase, legumain. Autophagy 7:1011-1027

[56] Yang H, Cho ME, Li TW, Peng H, Ko KS, Mato JM, Lu SC (2013) MicroRNAs regulate methionine adenosyltransferase 1A expression in hepatocellular carcinoma. J Clin Invest 123:285-298

[57] Jakubowski H (1999) Protein homocysteinylation: possible mechanism underlying pathological consequences of elevated homocysteine levels. FASEB J 13:2277-2283

[58] Jakubowski H (2004) Molecular basis of homocysteine toxicity in humans. Cell Mol Life Sci 61:470-487

[59] Xu L, Chen J, Gao J, Yu H, Yang P (2015) Crosstalk of homocysteinylation, methylation and acetylation on histone H3. Analyst 140:3057-3063 doi: 10.1039/c4an02355b.

[60] Jeffery CJ (1999) Moonlighting proteins. Trends Biochem Sci 24:8-11

7. FIGURE LEGENDS

Fig. 1. Endogenous expression and subcellular localization of BHMT. (a) Representative confocal microscopy images of rat hepatoma H35 cells incubated with preimmune or anti-BHMT sera (bar scale 20 μm). Colocalization with Hoechst 33342 nuclear staining is indicated in white. The cytoplasmic to nuclear signal (C/N) ratio was quantified (N=600) and the results are shown in the histogram. **(b)** Representative western blots of cytoplasmic (C) and nuclear (N) fractions from H35 cells; α-tubulin and lamin B1 signals are used as indicators for the absence of crosscontamination between cytoplasmic and nuclear fractions, respectively. The molecular weight of the markers appears on the left, whereas the size of the proteins is indicated on the right side of the panel. Results correspond to four independent experiments carried out at least in cuadruplicate.

Fig. 2. Analysis of tagged-BHMTs by western blotting. FLAG- and EGFP-tagged BHMT were overexpressed in *E. coli* and bacterial lysates analyzed by western blotting using anti-BHMT. The figure shows typical results of the mobility of wild-type BHMT (15 μg), BHMT-EGFP (15 μg) and FLAG-BHMT (15 μg) on a 10% SDS-PAGE gel; the calculated protein size is indicated on the right side of each image. The molecular weight of the markers is stated on the left.

Fig. 3. Analysis of BHMT subcellular localization by confocal microscopy. Overexpression of tagged BHMTs and the corresponding controls, FLAG and EGFP, was carried out in N2a, CHO, COS-7 and H35 cells. Subcellular distribution was evaluated by confocal microscopy. **(a)** Representative images for EGFP and BHMT-EGFP. **(b)** Representative results for FLAG and FLAG-BHMT. Colocalization with Hoechst 33342 nuclear staining is shown in white (bar scale 10 μm). Quantification of the fluorescent signal in cytoplasmic and nuclear compartments was performed using

the Leica confocal software. **(c)** Histograms depict the C/N signal ratio for EGFP and BHMT-EGFP. **(d)** Histograms show the C/N signal ratio for FLAG-BHMT. The C/N ratio (N >200) was calculated and the cells divided in three groups: C>N with ratios >1.2; C=N with ratios 1.0 ± 0.2; and C<N with ratios <0.8. The results correspond to a minimum of three independent experiments carried out in triplicate.

Fig. 4. Subcellular distribution of BHMT in a doxycycline inducible clone. **(a)** Representative confocal microscopy images of a CHO tet-ON BHMT-EGFP stable clone upon induction with the indicated concentrations of doxycycline (bar scale 20 μm). Colocalization with Hoechst 33342 nuclear staining is indicated in white. Results correspond to three independent experiments carried out in triplicate. **(b)** Representative fluorescence profiles of cells shown in panel a treated with different doxycycline doses, as indicated. **(c)** Induction of BHMT-EGFP expression in cytosolic fractions (50 μg/lane) upon stimulation with doxycycline (0-4 μg/ml) analyzed by western blotting using anti-BHMT; liver cytoplasm is included as positive control. The molecular weight of the markers appears on the left and the size of the proteins is indicated on the right side of the panel. The results shown are representative of four independent experiments carried out at least in triplicate.

Fig. 5. Expression levels and BHMT localization in rat tissues. (a) *Bhmt* expression in several rat tissues as assessed by real-time RT-PCR using the *Rn18s* gene as reference (N=3). For graphical purposes the fold change was established using the testis signal as reference. The upper right images show representative western blotting of cytosolic fractions obtained from the indicated rat tissues (N=3). For comparison 80 μg/lane were loaded from each tissue sample except liver (15 μg) and two exposures of the film are shown, long=30 min and short=1 min. The position of the 49 kDa marker is indicated at the left side of the images. All measurements were carried out in triplicate.

(b) BHMT immunohistological detection in rat tissues (N=6) using paraffin sections (5 μm) incubated with rabbit preimmune serum (A, C, E, G, I, K) or anti-BHMT (B, D, F, H, J, L). The figure shows representative images of liver (A, B), heart (C, D), cerebellum (E, F), kidney (G, H), testis (I, J), pancreas (K, L). Symbols indicate: Positive hepatocyte nuclei (arrowheads); hepatic centrilobular vein (v); cerebellum Purkinje neurons (arrowheads), granular layer (gl) and molecular layer (ml); negative kidney glomeruli (arrowheads); positive Sertolli cells of the testis (arrowheads); pancreatic acini cells (ap) and Langerhans islets (IL). Scale bar 10 μm (all tissues) and 50 μm (kidney).

Fig. 6. BHMT in subcellular fractions of normal rat liver. Livers of normal rats (N=6) were immediately processed for subcellular fractionation: cytoplasm (Cyt), washing step (S8), nucleus (Nuc). Cross-contamination between nuclear and cytoplasmic fractions was ruled out by LDH activity (<0.1 %) and western blotting using anti-α-tubulin and anti-lamin B1. **(a)** Representative western blots of the subcellular fractions. The molecular weight of the markers appears on the left side of the panel. **(b)** BHMT specific activities (mean ± SEM) in subcellular fractions measured in triplicate. **(c)** Representative gel filtration profile of nuclear BHMT detected by dot-blot analysis of the fractions (210 μl) using anti-BHMT. Standards used for column calibration were: Blue dextran (7.8 ml); apoferritin (9.85 ml); β-amylase (10.62 ml); alcohol dehydrogenase (11.34 ml); conalbumin (12.78 ml); ovalbumin (13.3 ml); carbonic anhydrase (14 ml); ATP (17.65 ml).

Fig. 7. Effects of D-galactosamine treatment on subcellular distribution of BHMT analyzed by confocal microscopy. (a) Representative confocal microscopy images of rat hepatoma H35 cells incubated with anti-BHMT or the corresponding preinmune serum after 48 hours of incubation in the presence of PBS or D-

galactosamine (bar scale 20 μm); colocalization with Hoechst staining is indicated in white. **(b)** Quantification of the cytoplasmic to nuclear signal ratio (C/N; N=600) of endogenous BHMT using the Leica confocal software. According to their C/N ratios, cells were divided in three groups: C>N with ratios >1.2; C=N with ratios 1.0 ± 0.2; and C<N with ratios <0.8. **(c)** Representative confocal images of H35 cells overexpressing EGFP or BHMT-EGFP after incubation with PBS or D-galactosamine (bar scale 15 μm). **(d)** Quantification of the cytoplasmic to nuclear signal ratio (N=150) in pEGFP and pBHMT-EGFP transfected cells. *p≤0.05.

Fig. 8. Evaluation of galactosamine-induced alterations in the subcellular distribution by western blotting and immunohistochemistry. (a) Representative western blot images of cytosols and nuclear fractions from control and galactosamine-treated H35 cells. The molecular weight of the markers is indicated on the side of each panel. Histograms depict results of the densitometric analysis of six independent experiments carried out in triplicate (*p≤0.05). Lamin B1 and α-tubulin signals were used as reference for nuclear and cytosolic fractions, respectively. **(b)** Representative images of paraffin sections (5 μm) of control (A, B, E, F; N=6) and Gal-treated livers (C, D, G, H; N=6) incubated with anti-BHMT (A-D) and preimmune (E-H) sera. Areas corresponding to the centrolobulillar vein (v) and the portal zones (p) are illustrated, where hepatocytes with positive nuclear staining (arrowheads) are indicated. Scale bar: 10 μm.

Fig. 9. BHMT in subcellular fractions of livers from control and galactosamine treated rats. Normal rats received two i.p. injections of PBS (control; N=13) or D-galactosamine (Gal; N=12) before sacrifice. Livers were excised and immediately processed for subcellular fractionation. **(a)** BHMT specific activity (mean ± SEM) measured in triplicate in nuclear and cytosolic samples (*p≤0.05). Cross-

contamination between nuclear and cytoplasmic fractions was <0.1% according to LDH activity. **(b)** Representative western blots of nuclear fractions of control (N= 5) and Gal-treated (N=5) livers incubated with anti-Hcy and anti-lamin B1. The size of the standards and the lamin B1 band are indicated on the left. **(c)** Representative western blots of cytoplasmic and nuclear fractions of the control and treated groups. The molecular weight of the markers is indicated at the center of the panel. Histograms show the mean ± SEM of the BHMT ratio to the specific markers, tubulin (cytoplasm) and lamin B (nucleus), quantified by densitometric scanning of the signals (*$p \leq 0.05$). **(d)** Representative analytical gel filtration profiles of nuclear BHMT elution analyzed by dot-blot using anti-BHMT. The elution volume of the markers was: Blue dextran (7.8 ml); apoferritin (9.85 ml); β-amylase (10.62 ml); alcohol dehydrogenase (11.34 ml); conalbumin (12.78 ml); ovalbumin (13.3 ml); carbonic anhydrase (14 ml); ATP (17.65 ml).

Fig. 10. Evaluation of glutathione concentrations and apoptosis in H35 cells after treatment with agents inducing subcellular redistribution of BHMT. (a) GSH levels in H35 cells treated with PBS (control), D-galactosamine (Gal), N-acetylcysteine (NAC), S-adenosylmethionine (AdoMet), buthionine sulfoximine (BSO), ethyl ester of glutathione (EGSH) and combinations of these agents. The results (mean ± SEM) depicted correspond to a representative experiment out of three carried out in triplicate and were considered significant when $p \leq 0.05$ as compared to control cells (^{a}), Gal-treated cells (^{b}) or BSO-treated cells (^{c}). **(b)** GSH/GSSG ratios in H35 receiving the treatments specified in panel a. Results (mean ± SEM) were considered significant when $p \leq 0.05$ as compared to control cells (^{a}), Gal-treated cells (^{b}) or BSO-treated cells (^{c}). **(c)** Representative western blots of the treated cells incubated with anti-caspase-3

and anti-tubulin; six independent experiments were analyzed. The size of the standards, as well as the size of α-tubulin, are indicated on the left side of the panels.

Fig. 11. BHMT distribution is regulated by changes in glutathione levels. (a) H35 cells were treated with 10 mM D-galactosamine for 48 hours or **(b)** 1 mM BSO for 24 hours, the cytoplasmic and nuclear fractions isolated and changes in BHMT distribution analyzed by western blotting. The preventive effects of 5 mM NAC, 0.5 mM AdoMet or 1 mM EGSH were also explored. **(a, b)** Changes induced in BHMT cytoplasmic levels. **(c, d)** Effects on nuclear protein levels. The figure shows representative western blots of six experiments carried out in duplicate. The molecular weight of the markers is indicated at the left side of the images. Quantification was carried out by densitometric scanning and the BHMT/tubulin or BHMT/lamin B1 ratios calculated. Histograms depict the mean ± SEM of the percentages of variation calculated against the corresponding H35 control cells (100%). $^{a}p<0.05$ vs. control; $^{b}p<0.05$ vs. D-galactosamine or BSO.

Fig. 12. Effect of acute acetaminophen intoxication on the subcellular distribution of hepatic BHMT. Rats received i.p. injection of PBS (C; N=6) or 250 mg/kg acetaminophen (APAP; N=6) 24 hours before sacrifice. Subcellular fractions of the livers were obtained and analyzed. **(a)** Representative western blots of cytoplasmic and nuclear fractions of the control and treated groups. The molecular weight of the markers is indicated at side of each image. Histograms show the mean ± SEM of the BHMT ratio to the specific markers, tubulin (cytoplasm) and lamin B1 (nucleus), quantified by densitometric scanning of the signals ($*p\leq0.05$). **(b, c)** Representative analytical gel filtration profiles analyzed by dot-blot using anti-BHMT of cytosolic **(b)** and nuclear **(c)** fractions of control rats. **(d, e)** Representative analytical gel filtration profiles analyzed by dot-blot using anti-BHMT of cytosolic **(d)** and nuclear **(e)** fractions

of APAP-treated animals. The elution volume of the markers was: Blue dextran (7.8 ml); apoferritin (9.85 ml); β-amylase (10.62 ml); alcohol dehydrogenase (11.34 ml); conalbumin (12.78 ml); ovalbumin (13.3 ml); carbonic anhydrase (14 ml); ATP (17.65 ml).

Fig. 13. Rat BHMT sequence and localization of residues putatively involved in subcellular distribution. (a) Two views of the BHMT molecular surface prepared using PyMOL and data of the rat crystal structure (1UMY). Residues K10 and R11 are shown as sticks (left) and the position of L235 and L240 with high NES scores (>0.5) is indicated on the right. **(b)** Rat BHMT sequence where the following features are indicated: the basic N-terminal residues (green box); the putative NES leucine residues (yellow boxes); and the two point mutations (blue) previously described in our mRNA. **(c)** BLASTP alignment of rat and human BHMT N-terminal sequences. Basic residues of interest are shown in a green box.

Fig. 14. Purified BHMT mutants analyzed by western blotting. The mutants were purified on chitin beads and their behavior analyzed by western blotting with anti-BHMT. Samples of the purified mutants and wild type BHMT (7 μg) were run in parallel for comparison. The molecular weight of the markers is indicated on the left. The figure shows a representative image of the three independent experiments carried out.

Fig. 15. Subcellular localization changes in BHMT mutants overexpressed in H35 cells. (a) Representative confocal microscopy images of rat hepatoma H35 cells transiently transfected with pEGFP (control) or pBHMT-EGFP plasmids carrying N-terminal mutations (N=200) of three independent experiments carried out in triplicate. **(b)** Representative immunofluorescence images obtained with the FLAG-tagged mutants (N=200) of three independent experiments carried out in triplicate.

Colocalization with Hoechst 33342 nuclear staining is shown in white (bar scale 10 μm). **(c)** Quantification of the EGFP fluorescence signals in the cytoplasm (C) and nuclear compartments (N) and the C/N ratio with the Leica confocal software (N≥200). **(d)** Quantification of the subcellular distribution for FLAG-BHMT and the mutants (N≥200). Cells were divided in three groups for their classification: C>N with ratios >1.2; C=N with ratios 1.0 ± 0.2; and C<N with ratios <0.8. The results shown (mean ± SEM) correspond to a minimum of three independent experiments carried out in triplicate. *p≤0.05.

TABLE 1

Activity and association state of the tagged-BHMTs expressed in *E. coli* BL21(DE3).

plasmid	protein	Specific activity[a,d] (nmol/min/mg)	Specific activity[b] (nmol/min/AU)	Association state[e]
	Purified BHMT[c]	12.15 ± 1.39	0.94 ± 0.11	Tetramer
pFLAG-BHMT	FLAG-BHMT	0.91 ± 0.21	1.57 ± 0.37	Tetramer
pT7.7-BHMT-EGFP	BHMT-EGFP	0.71 ± 0.06	1.74 ± 0.14	Tetramer

[a]Activity was measured in the cytosol of bacteria transformed with the specified plasmids and the specific activity calculated using the total protein concentration.
[b]Specific activity was calculated using the densitometric value of the BHMT specific band obtained by immunoblotting of the samples.
[c]Activity of purified BHMT (75 μl) was measured for comparison.
[d] The table shows results of a typical experiment carried out in triplicate (mean ± SD).
[e]Cytosols (100 μl) were analyzed by analytical gel filtration chromatography and elution of the proteins was followed by A_{280} and dot-blot.

TABLE 2

Immunohistochemical staining and subcellular localization.

	Anti-BHMT signal[b]		
Organ/tissue type[a]	**Stucture/cell type**	**cytoplasm**[c]	**nucleus**[c]
Liver	Hepatocyte	+	+
Brain	Cerebellar Purkinje cells	+	+
Kidney	Epithelium of proximal convoluted tubules	+	+
	Glomeruli	-	-
Testis	Spermatogenic epithelium	-	-
	Sertolli cells	+	+
Digestive system	Mucosa	-	+
Pancreas	Pancreatic acini cells	+	-
	Langerhans islets	+	+
Heart	Muscle cells	+	-
Skeletal muscle	Muscle cells	+	-
Blood vessels	Endothelium	-	-
Smooth muscle	Visceral and vascular wall	-	-
Connective tissue	Visceral and vascular wall	-	-

[a]Tissues were obtained from adult Wistar rats (N=3) and immediately fixed with formaldehyde.
[b]Sections of the tissues were incubated with anti-BHMT or preimmune anti-sera and developed with EnVision.
[c]Positive (+) and negative (-) staining for BHMT in relevant cell types and subcellular localization of the signal.

TABLE 3

Activity of the purified recombinant BHMT mutants.

Purified protein	Specific activity[a,c] (nmol/min/mg)	Association state[b,c]
BHMT	12.15 ± 1.39	Tetramer
BHMT-K7A	10.9 ± 1.00	Tetramer
BHMT-K8A	4.74 ± 0.36	Tetramer
BHMT-K10A	4.36 ± 1.22	Tetramer

[a]BHMT activity (75 μl) was measured in triplicate and the specific activities calculated (mean ± SD).
[b]Samples of the purified proteins (100 μl) were analyzed by analytical gel filtration chromatography and the elution volume determined by A_{280} and dot-blot.
[c]The table shows results of a typical experiment out of three carried out in triplicate.

a

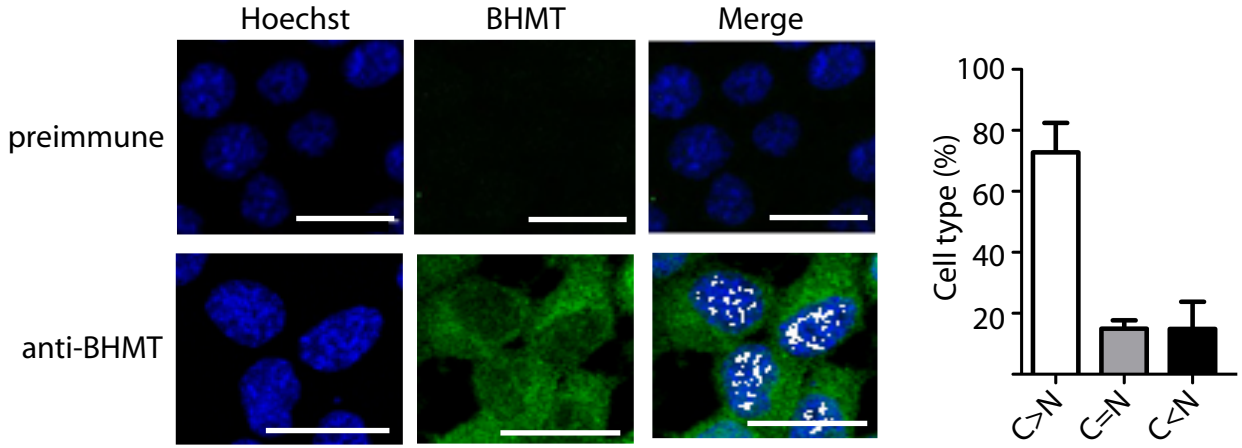
Hoechst
BHMT
Merge
preimmune
anti-BHMT
100
80
60
40
20
Cell type (%)
C>N
C=N
C<N

b

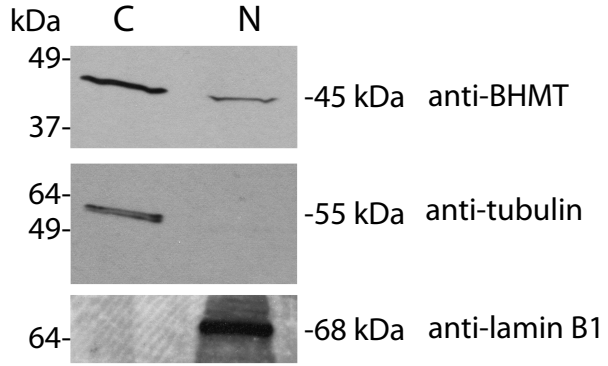
kDa
C
N
49-
37-
-45 kDa
anti-BHMT
64-
49-
-55 kDa
anti-tubulin
64-
-68 kDa
anti-lamin B1

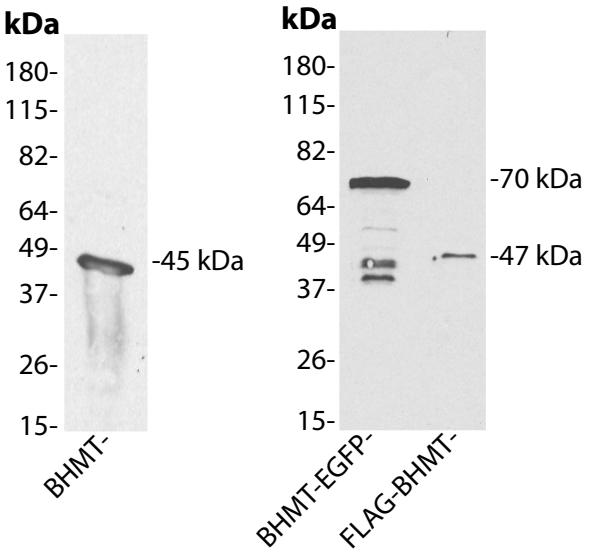
kDa
180-
115-
82-
64-
49-
37-
26-
15-
-45 kDa
BHMT-
kDa
180-
115-
82-
64-
49-
37-
26-
15-
-70 kDa
-47 kDa
BHMT-EGFP-
FLAG-BHMT-

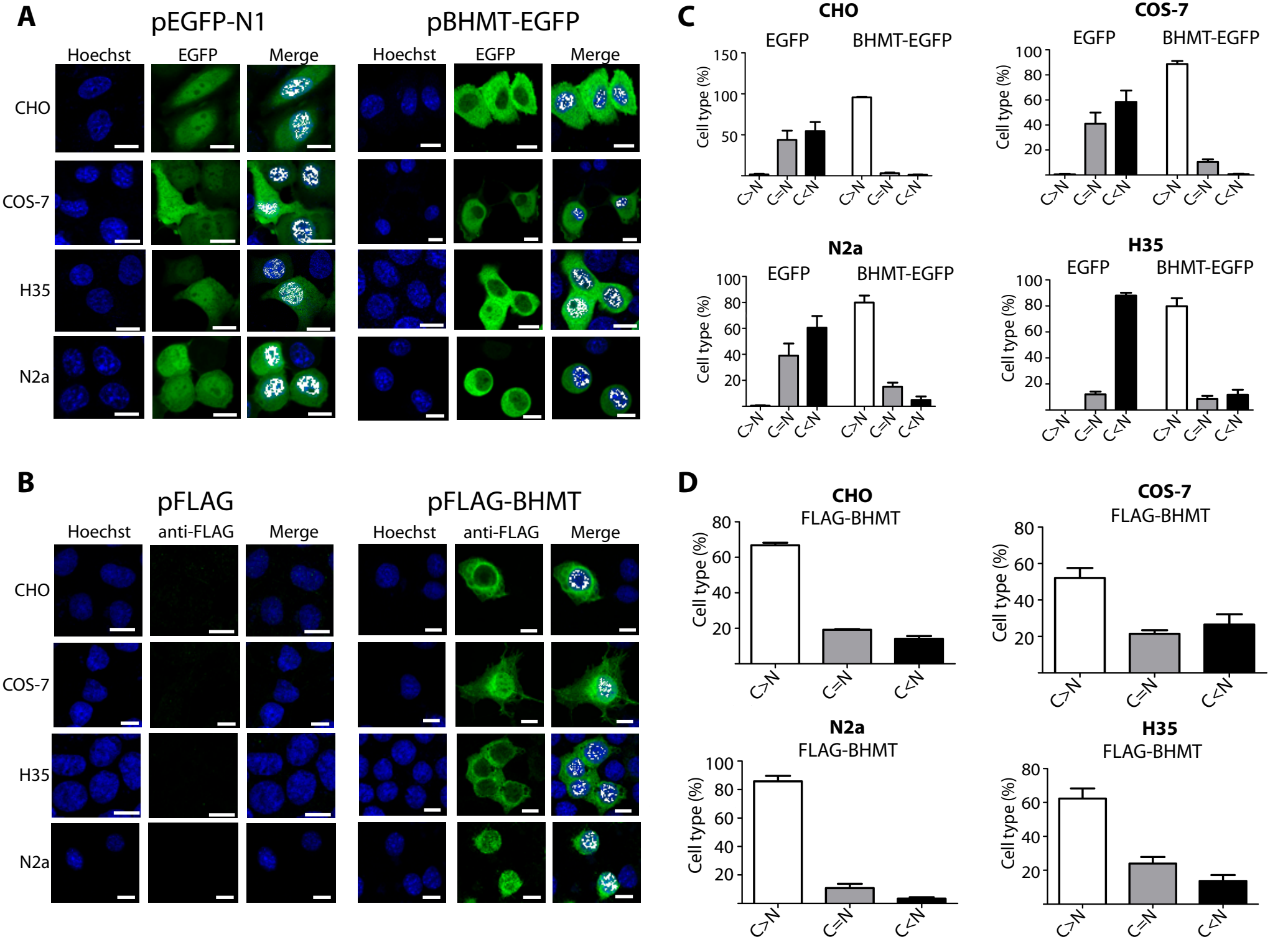
A
pEGFP-N1
pBHMT-EGFP
Hoechst
EGFP
Merge
CHO
COS-7
H35
N2a
B
pFLAG
pFLAG-BHMT
Hoechst
anti-FLAG
Merge
C
CHO
COS-7
N2a
H35
EGFP
BHMT-EGFP
Cell type (%)
C>N
C=N
C<N
D
FLAG-BHMT

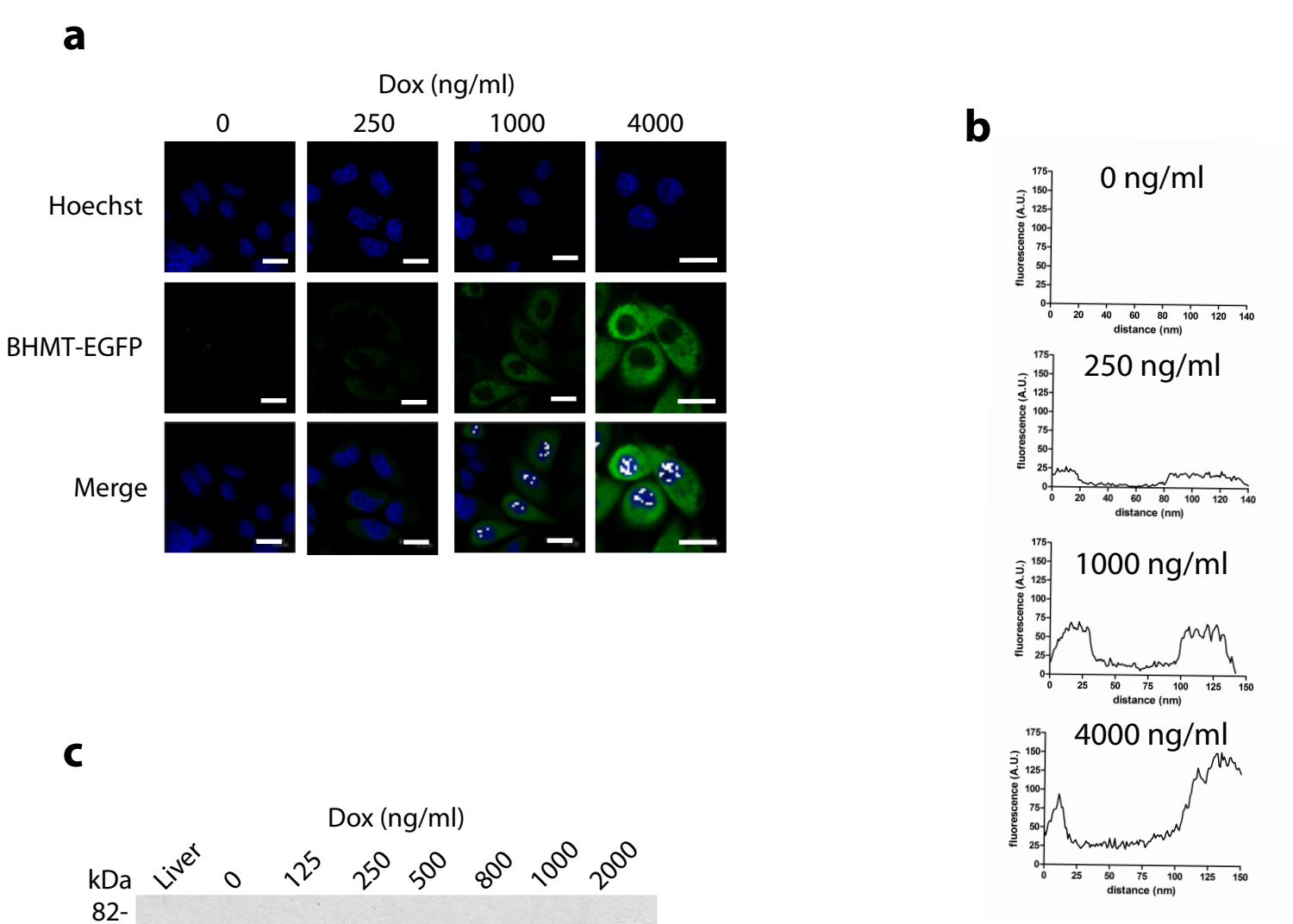
a
Dox (ng/ml)
0
250
1000
4000
Hoechst
BHMT-EGFP
Merge
b
0 ng/ml
250 ng/ml
1000 ng/ml
4000 ng/ml
fluorescence (A.U.)
distance (nm)
c
Dox (ng/ml)
kDa
Liver
0
125
250
500
800
1000
2000
82-
64-
49-
- 70 kDa BHMT-EGFP
- 45 kDa BHMT

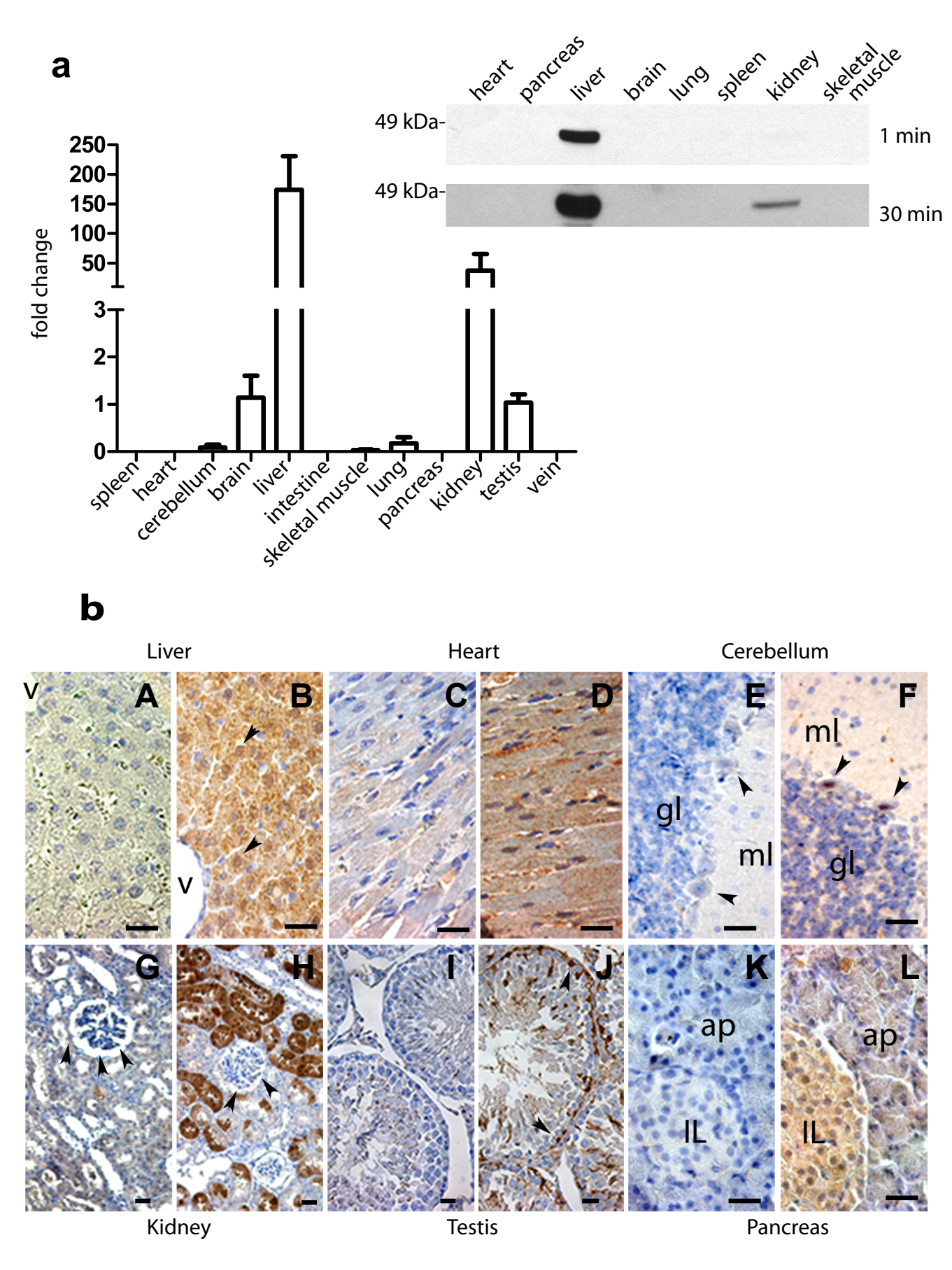
a
heart
pancreas
liver
brain
lung
spleen
kidney
skeletal muscle
49 kDa-
1 min
49 kDa-
30 min
fold change
250
200
150
100
50
3
2
1
0
spleen
heart
cerebellum
brain
liver
intestine
skeletal muscle
lung
pancreas
kidney
testis
vein
b
Liver
Heart
Cerebellum
A
B
C
D
E
F
V
V
gl
ml
ml
gl
G
H
I
J
K
L
ap
IL
ap
IL
Kidney
Testis
Pancreas

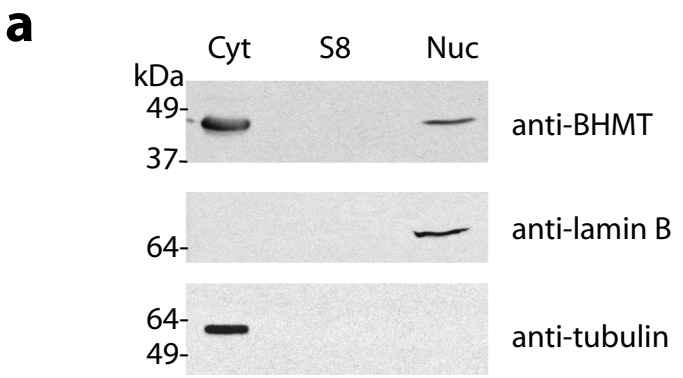
a
Cyt
S8
Nuc
kDa
49-
37-
anti-BHMT
64-
anti-lamin B
64-
49-
anti-tubulin

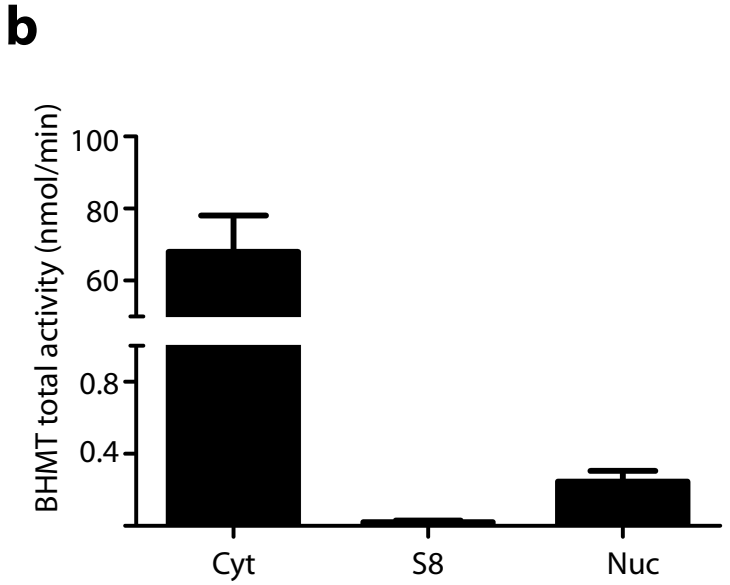
b
BHMT total activity (nmol/min)
100
80
60
0.8
0.4
Cyt
S8
Nuc

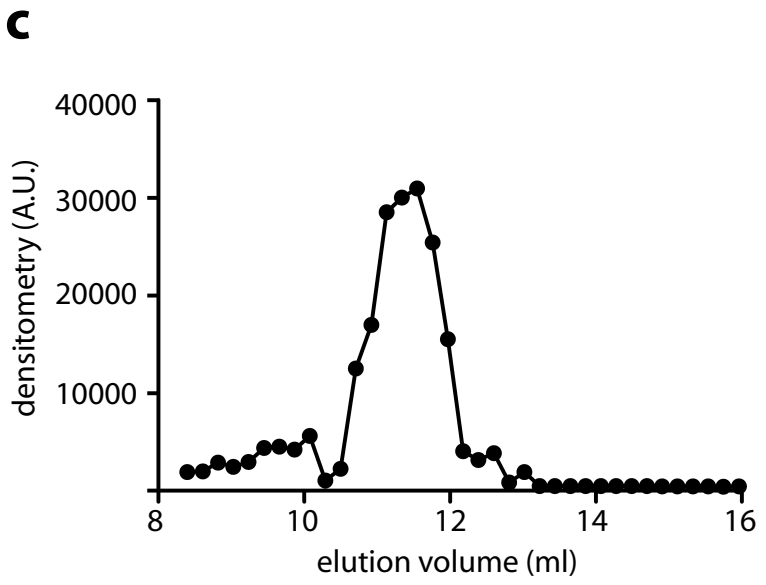
c
densitometry (A.U.)
40000
30000
20000
10000
8
10
12
14
16
elution volume (ml)

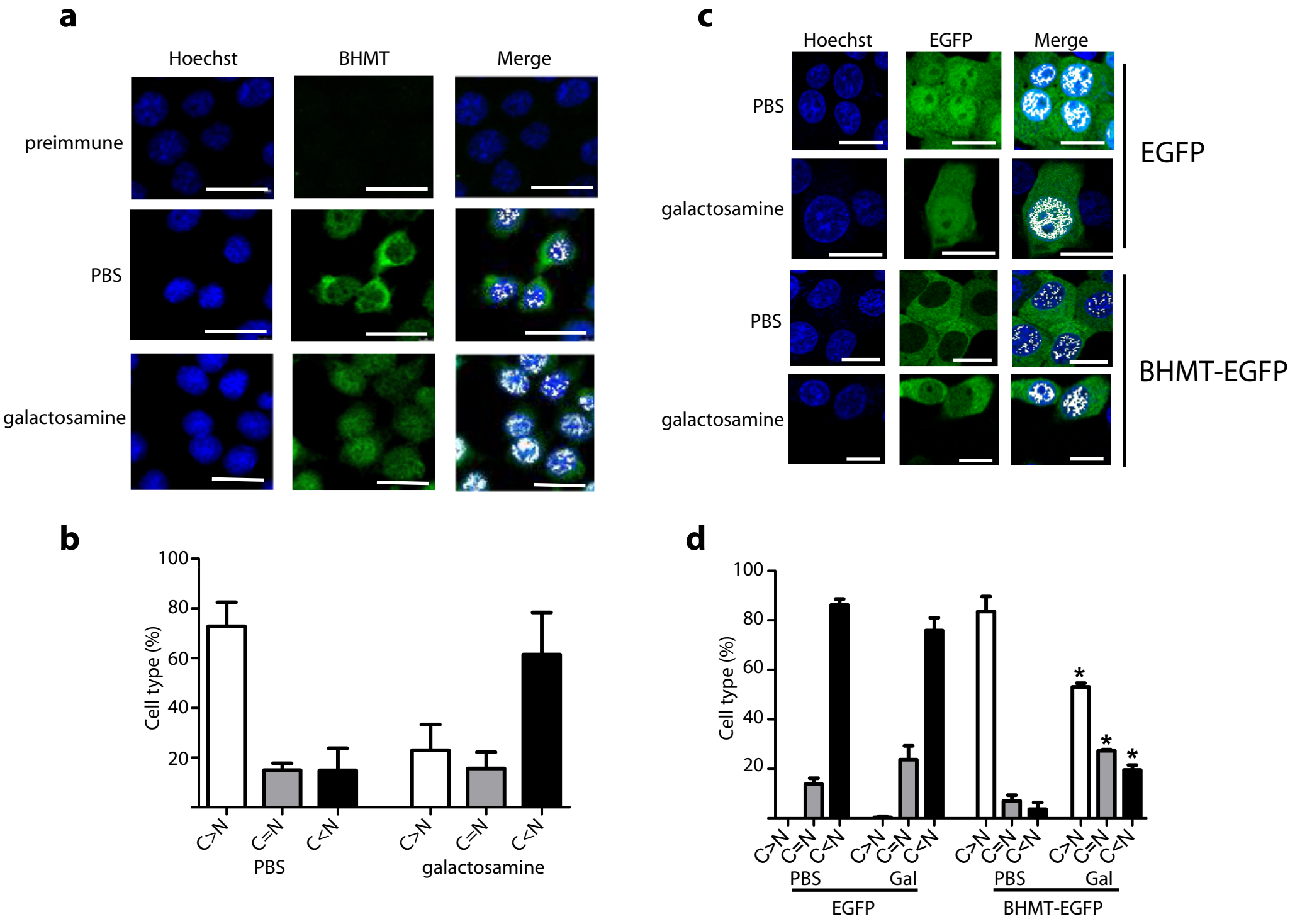
a
Hoechst
BHMT
Merge
preimmune
PBS
galactosamine
c
Hoechst
EGFP
Merge
PBS
galactosamine
EGFP
PBS
galactosamine
BHMT-EGFP
b
Cell type (%)
100
80
60
40
20
C>N
C=N
C<N
PBS
galactosamine
d
Cell type (%)
100
80
60
40
20
C>N
C=N
C<N
PBS
Gal
EGFP
BHMT-EGFP
*

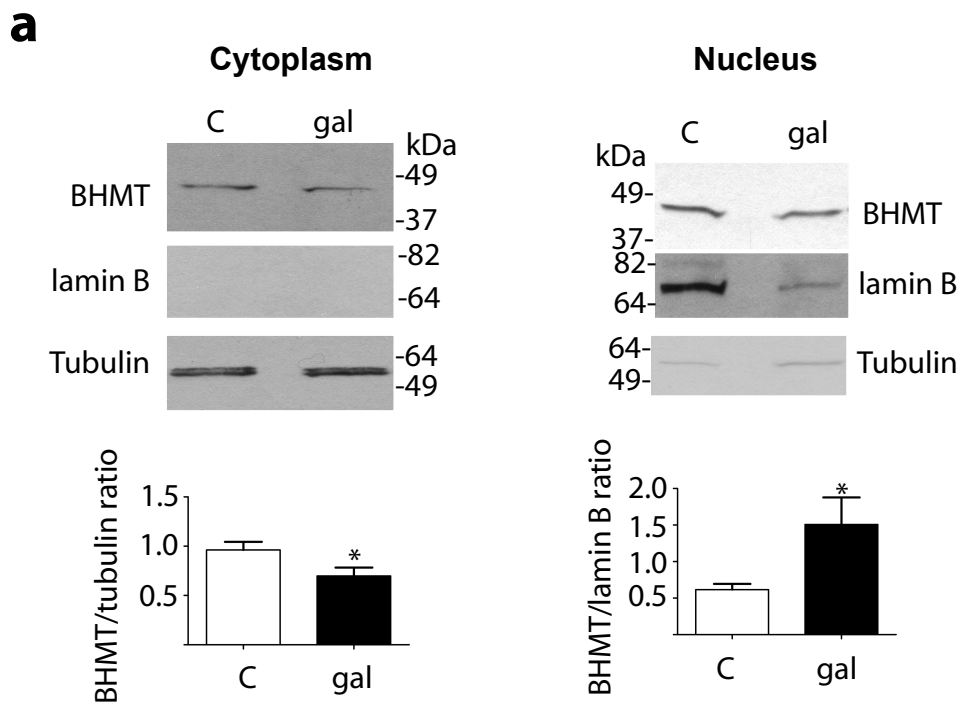
a
Cytoplasm
Nucleus
C
gal
kDa
BHMT
lamin B
Tubulin
-49
-37
-82
-64
-64
-49
49-
37-
82-
64-
64-
49-
BHMT/tubulin ratio
BHMT/lamin B ratio
1.5
1.0
0.5
2.0
1.5
1.0
0.5
*
C
gal

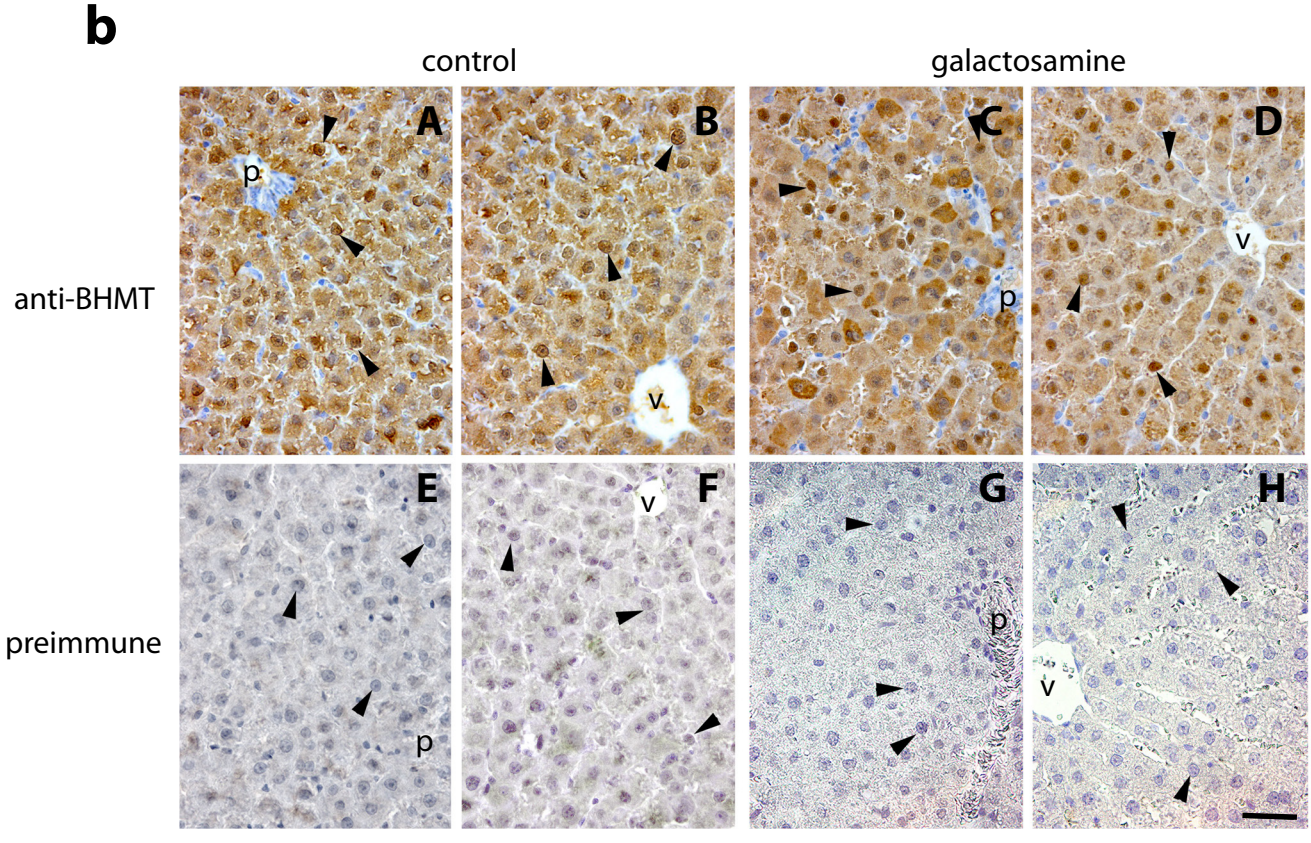
b
control
galactosamine
anti-BHMT
preimmune
A
B
C
D
E
F
G
H
p
v

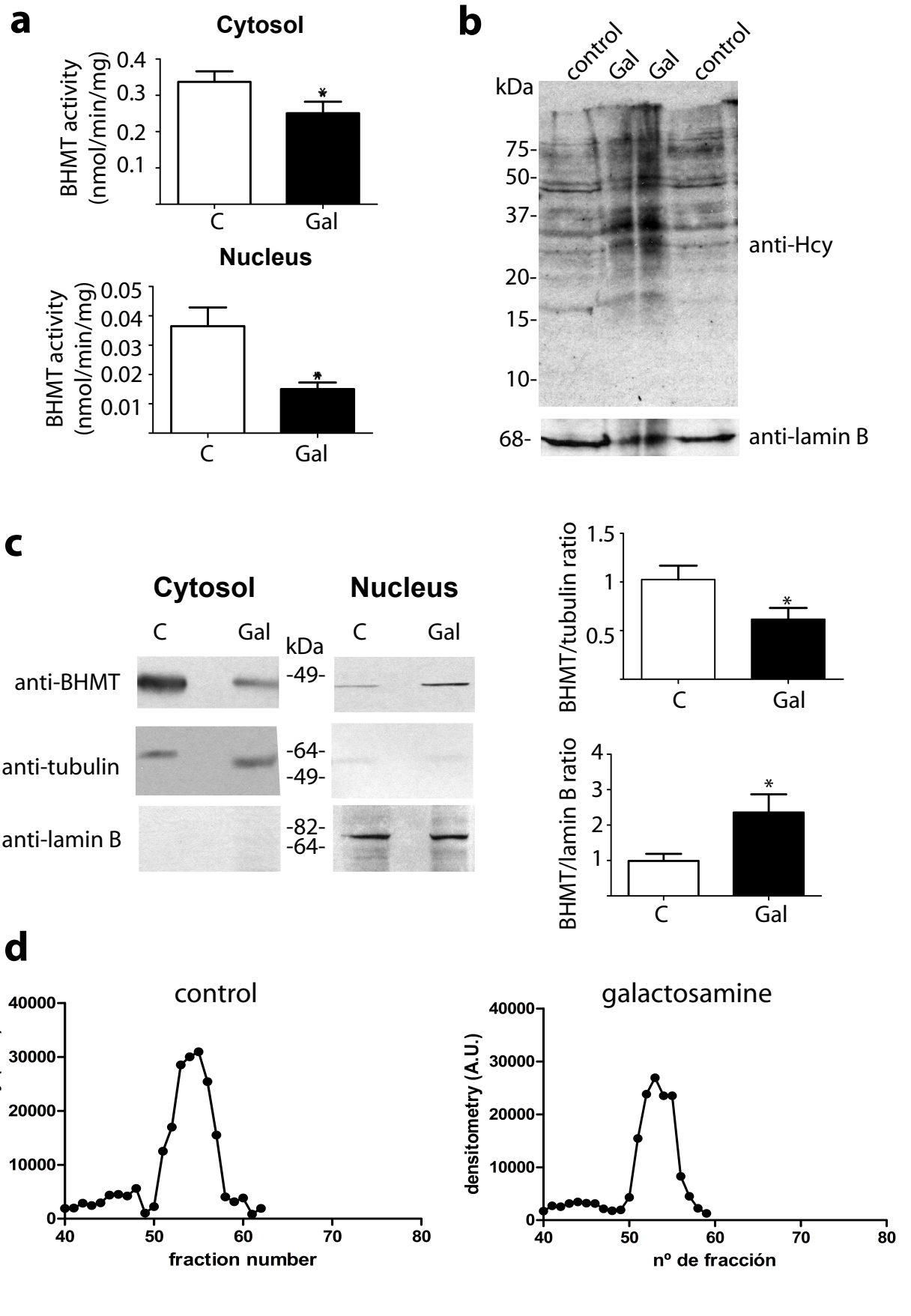
a
Cytosol
BHMT activity (nmol/min/mg)
0.4
0.3
0.2
0.1
C
Gal
Nucleus
BHMT activity (nmol/min/mg)
0.05
0.04
0.03
0.02
0.01
C
Gal
b
control
Gal
Gal
control
kDa
75-
50-
37-
20-
15-
10-
anti-Hcy
68-
anti-lamin B
c
Cytosol
Nucleus
C
Gal
kDa
C
Gal
anti-BHMT
-49-
anti-tubulin
-64-
-49-
anti-lamin B
-82-
-64-
BHMT/tubulin ratio
1.5
1
0.5
C
Gal
BHMT/lamin B ratio
4
3
2
1
C
Gal
d
control
densitometry (A.U.)
40000
30000
20000
10000
0
40
50
60
70
80
fraction number
galactosamine
densitometry (A.U.)
40000
30000
20000
10000
0
40
50
60
70
80
nº de fracción

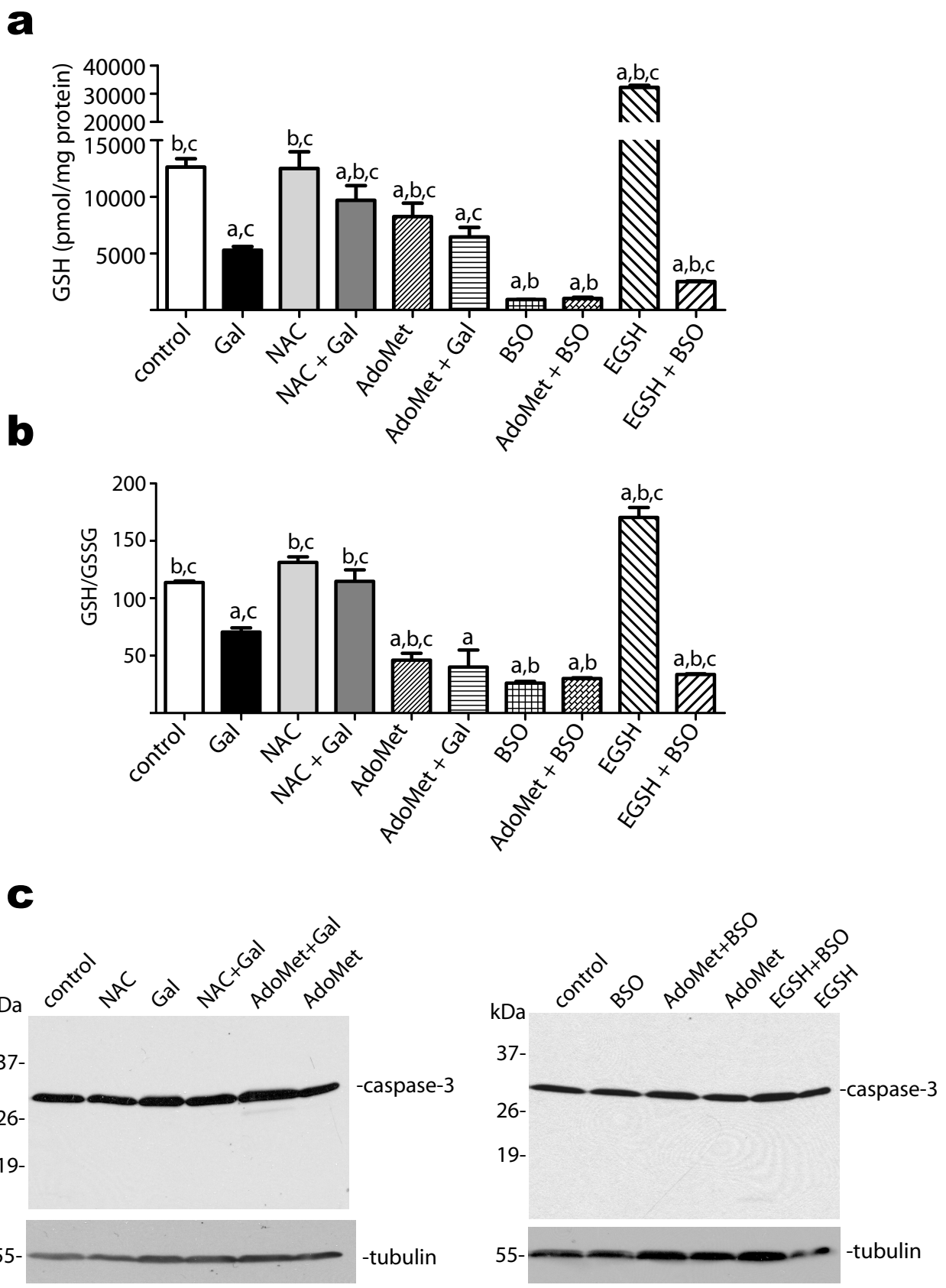
a
GSH (pmol/mg protein)
40000
30000
20000
15000
10000
5000
b,c
a,c
b,c
a,b,c
a,b,c
a,c
a,b
a,b
a,b,c
a,b,c
control
Gal
NAC
NAC + Gal
AdoMet
AdoMet + Gal
BSO
AdoMet + BSO
EGSH
EGSH + BSO
b
GSH/GSSG
200
150
100
50
b,c
a,c
b,c
b,c
a,b,c
a
a,b
a,b
a,b,c
a,b,c
control
Gal
NAC
NAC + Gal
AdoMet
AdoMet + Gal
BSO
AdoMet + BSO
EGSH
EGSH + BSO
c
kDa
control
NAC
Gal
NAC+Gal
AdoMet+Gal
AdoMet
37-
26-
19-
-caspase-3
55-
-tubulin
kDa
control
BSO
AdoMet+BSO
AdoMet
EGSH+BSO
EGSH
37-
26-
19-
-caspase-3
55-
-tubulin

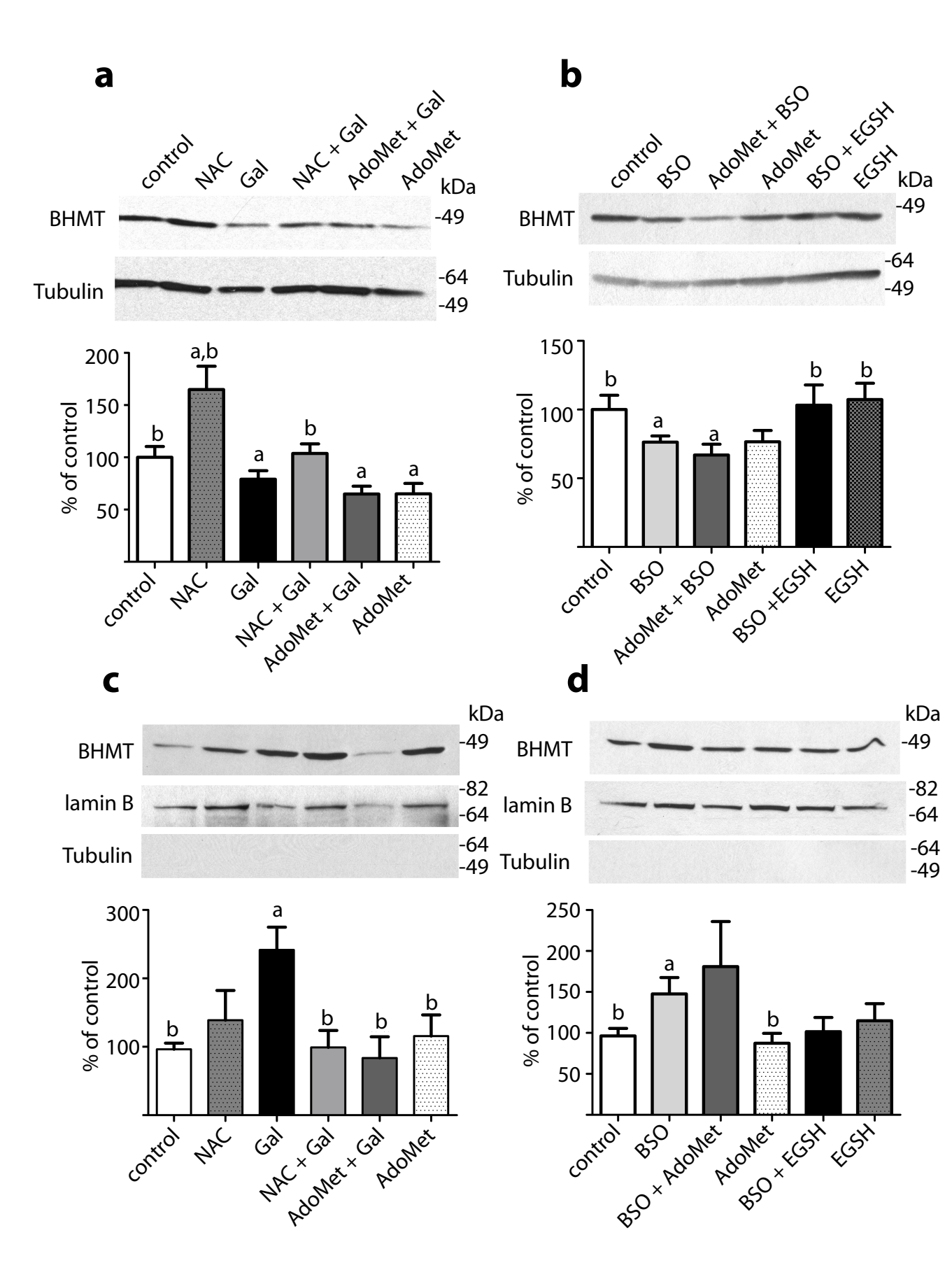
a
control
NAC
Gal
NAC + Gal
AdoMet + Gal
AdoMet
kDa
BHMT
-49
Tubulin
-64
-49
% of control
200
150
100
50
a,b
b
a
b
a
a
control
NAC
Gal
NAC + Gal
AdoMet + Gal
AdoMet
b
control
BSO
AdoMet + BSO
AdoMet
BSO + EGSH
EGSH
kDa
BHMT
-49
Tubulin
-64
-49
% of control
150
100
50
b
a
a
b
b
control
BSO
AdoMet + BSO
AdoMet
BSO +EGSH
EGSH
c
kDa
BHMT
-49
lamin B
-82
-64
Tubulin
-64
-49
% of control
300
200
100
b
a
b
b
b
control
NAC
Gal
NAC + Gal
AdoMet + Gal
AdoMet
d
kDa
BHMT
-49
lamin B
-82
-64
Tubulin
-64
-49
% of control
250
200
150
100
50
b
a
b
b
b
control
BSO
BSO + AdoMet
AdoMet
BSO + EGSH
EGSH

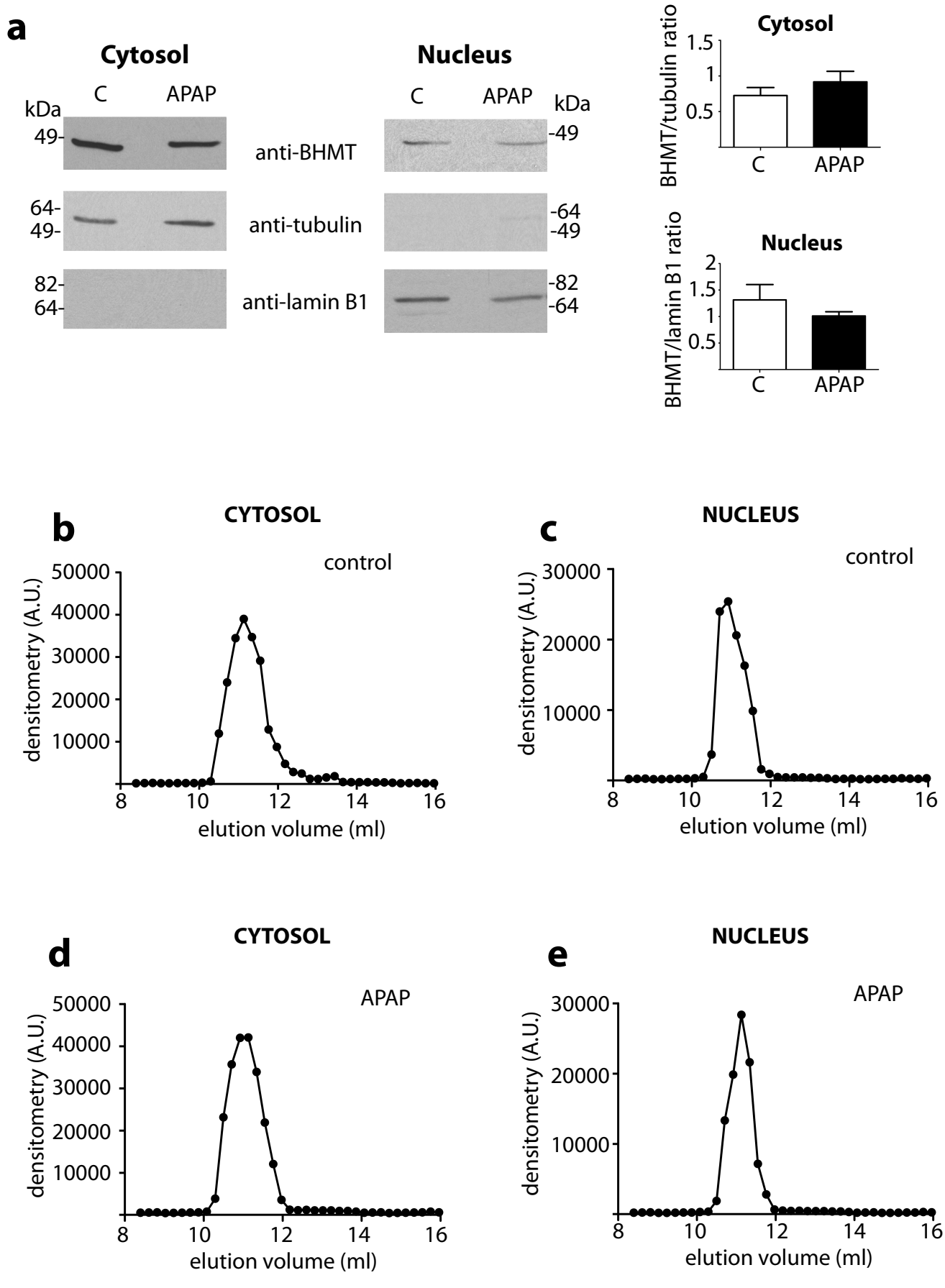
a
Cytosol
Nucleus
C
APAP
kDa
49-
64-
82-
anti-BHMT
anti-tubulin
anti-lamin B1
-49
-64
-82
Cytosol
BHMT/tubulin ratio
1.5
1
0.5
Nucleus
BHMT/lamin B1 ratio
2
b
CYTOSOL
control
densitometry (A.U.)
50000
40000
30000
20000
10000
8
10
12
14
16
elution volume (ml)
c
NUCLEUS
d
APAP
e

A

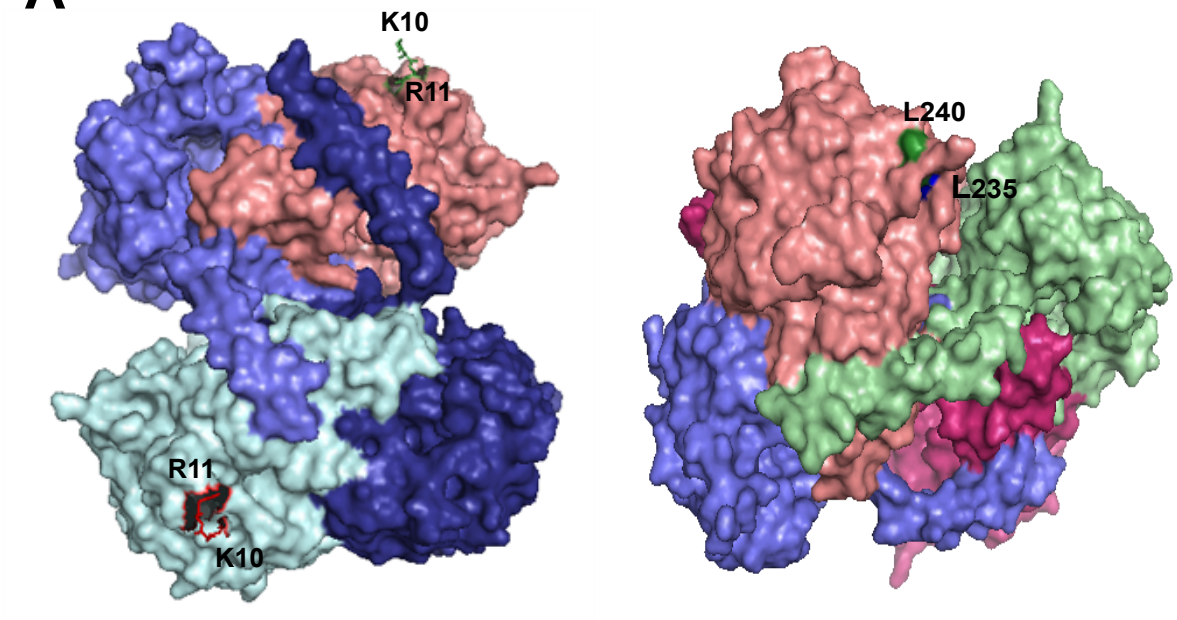

B

[1]MAPIAGKKAKRGILERLNAGEVVIGDGGFVFALEKRGYVKAGPWTPEAAV
[51]EHPEAVRQLHREFLRAGSNVMQTFTFYASEDKLENRGNYVAEKISGQKVN
[101]EAACDIARQVADEGDALVAGGVSQTPSYLSCKSETEVKKIFHQQLEVFMK
[151]KNVDFLIAEYFEHVEEAVWAVEALKTSGKPIAATMCIGPEGDLHGVSPGE
[201]CAVRLVKAGAAIVGVNCHFDPSTSLQTIKLMKEGLEAARLKAYLMSQPLA
[251]YHTPDCGKQGFIDLPEFPFGLEPRVATRWDIQKYAREAYNLGVRYIGGCC
[301]GFEPYHIRAIAEELAPERGFLPPASEKHGSWGSGLDMHTKPWIRARARKE
[351]YWQNLRIASGRPYNPSMSKPDAWGVTKGAAELMQQKEATTEQQLRALFEK
[401]QKFKSAQ

C

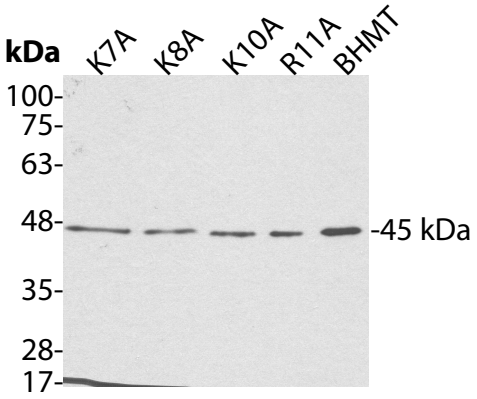
kDa
K7A
K8A
K10A
R11A
BHMT
100-
75-
63-
48-
35-
28-
17-
-45 kDa

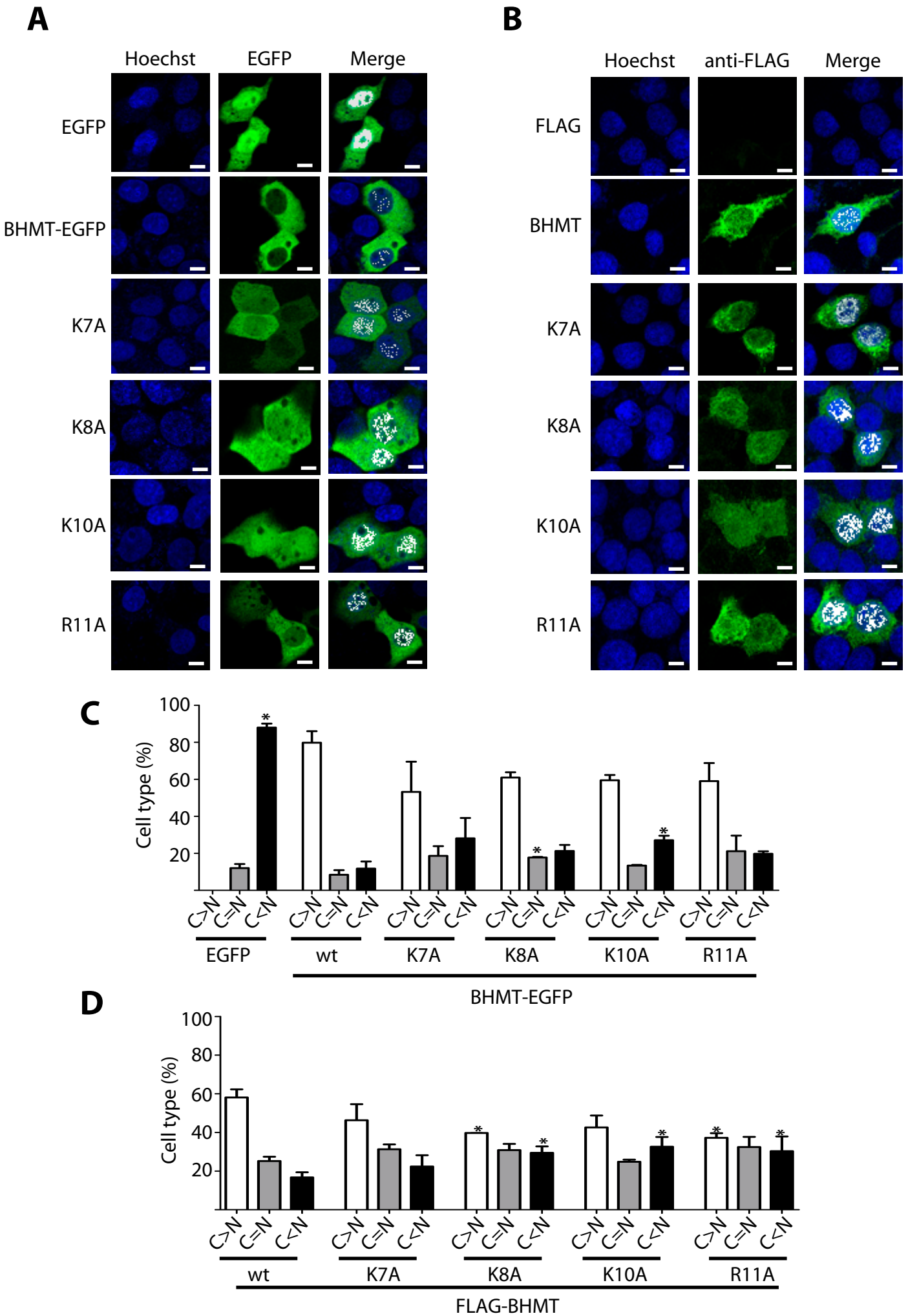
A
Hoechst
EGFP
Merge
EGFP
BHMT-EGFP
K7A
K8A
K10A
R11A
B
Hoechst
anti-FLAG
Merge
FLAG
BHMT
K7A
K8A
K10A
R11A
C
Cell type (%)
100
80
60
40
20
C>N
C=N
C<N
EGFP
wt
K7A
K8A
K10A
R11A
BHMT-EGFP
D
Cell type (%)
100
80
60
40
20
C>N
C=N
C<N
wt
K7A
K8A
K10A
R11A
FLAG-BHMT